

See discussions, stats, and author profiles for this publication at: <https://www.researchgate.net/publication/227855540>

Microrough Cobalt-Chromium Alloy Surfaces for Paclitaxel Delivery: Preparation, Characterization, and In Vitro Drug Release Studies

ARTICLE in LANGMUIR · JUNE 2012

Impact Factor: 4.46 · DOI: 10.1021/la301636z · Source: PubMed

CITATIONS

17

READS

33

3 AUTHORS, INCLUDING:



Sandeep Kakade

4 PUBLICATIONS 43 CITATIONS

[SEE PROFILE](#)



Gopinath Mani

Dr.NGP Institute of Technology

25 PUBLICATIONS 709 CITATIONS

[SEE PROFILE](#)

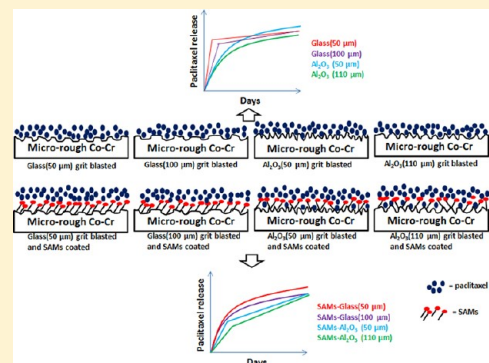
Microrough Cobalt–Chromium Alloy Surfaces for Paclitaxel Delivery: Preparation, Characterization, and *In Vitro* Drug Release Studies

Susan Lancaster, Sandeep Kakade, and Gopinath Mani*

Biomedical Engineering Program, The University of South Dakota, 4800 North Career Avenue, Sioux Falls, South Dakota 57107, United States

Supporting Information

ABSTRACT: Cobalt–chromium (Co–Cr) alloys have extensive biomedical applications including drug-eluting stents (DES). This study investigates the use of eight different microrough Co–Cr alloy surfaces for delivering paclitaxel (PAT) for potential use in DES. The eight different surfaces include four bare microrough and four self-assembled monolayer (SAM) coated microrough surfaces. The bare microrough surfaces were prepared by grit blasting Co–Cr with glass beads (50 and 100 μm in size) and Al₂O₃ (50 and 110 μm). The SAM coated surfaces were prepared by depositing a –COOH terminated phosphonic acid monolayer on the different microrough surfaces. PAT was then deposited on all the bare and SAM coated microrough surfaces. The surfaces were characterized using scanning electron microscopy (SEM), 3D optical profilometry, and Fourier transform infrared spectroscopy (FTIR). SEM showed the different morphologies of microrough surfaces without and with PAT coating. An optical profiler showed the 3D topography of the different surfaces and the changes in surface roughness and surface area after SAM and PAT deposition. FTIR showed ordered SAMs were formed on glass bead grit blasted surfaces, while the molecules were disordered on Al₂O₃ grit blasted surfaces. Also, FTIR showed the successful deposition of PAT on these surfaces. The PAT release was investigated for up to two weeks using high performance liquid chromatography. Al₂O₃ grit blasted bare microrough surfaces showed sustained release profiles, while the glass bead grit blasted surfaces showed burst release profiles. All SAM coated surfaces showed biphasic drug release profiles, which is an initial burst release followed by a slow and sustained release. SAM coated Al₂O₃ grit blasted surfaces prolonged the sustained release of PAT in a significant amount during the second week of drug elution studies, while this behavior was not observed for any other surfaces used in this study. Thus, this study demonstrates the use of different microrough Co–Cr alloy surfaces for delivering PAT for potential applications in DES and other medical devices.



1. INTRODUCTION

Cobalt–chromium (Co–Cr) alloys which belong to ASTM standards F75 (Co-28Cr-6Mo casting alloy), F799 (Co-28Cr-6Mo thermodynamically processed alloy), F90 (Co-20Cr-25W-10Ni wrought alloy), and F562 (Co-35Ni-20Cr-10Mo wrought alloy) have extensive applications in a variety of biomedical implants and devices including but not limited to cardiovascular stents, total hip replacements, artificial knee joints, shoulder and elbow prosthesis, dental restorations, removable partial dentures, and spinal fixation rods.¹ Co–Cr alloys have either a smooth or rough surface depending on the intended application. Microrough Co–Cr alloy surfaces enhance the osseointegration of orthopedic and dental implants.^{2–4} Osseointegration is a process in which the bone grows into the implant surface without the formation of fibrous tissue at the interface. Hence, the biomechanical stability of the implants is greatly improved by the microrough surfaces. Although a plethora of literature is available on the use of microrough Co–Cr alloy surfaces for improving the implant-tissue integration,^{2–4} the number of reports available on drug delivery from these alloy surfaces is rather limited.

Drug delivery from microrough Co–Cr alloy surfaces has tremendous potential applications in coronary artery stents. A stent is a small metal mesh tube that is implanted to open a blocked artery.^{5,6} However, the endothelial cell injury caused during stent implantation leads to a cascade of biological events resulting in neointimal hyperplasia, which is a pathological condition in which the smooth muscle cells grow inside the artery and reocclude it.⁷ Drug-eluting stents (DES) which deliver therapeutic drugs locally to prevent the growth of smooth muscle cells are currently used in patients.^{8,9} However, there are a few limitations associated with the use of currently available DES. Polymers are generally used to deliver drugs from stent surfaces. However, some polymers can cause serious adverse reactions including late stent thrombosis (LST), which is a condition in which blood clots occur in the arteries of patients after months or years of stent implantation.^{10–14} The clinical consequences of LST are catastrophic events including

Received: April 22, 2012

Revised: June 21, 2012

Published: June 22, 2012



ACS Publications

© 2012 American Chemical Society

11511

dx.doi.org/10.1021/la301636z | Langmuir 2012, 28, 11511–11526

heart attack and death. Hence, the research in this area is currently focused on developing more biocompatible polymers or a totally polymer-free approach to deliver drugs from stents. The study that we report here belongs to the latter category.

One of the earliest polymer-free drug delivery approaches developed was to coat the drug directly onto the 316 L stainless steel (316 L SS) stent surfaces by dip coating.¹⁵ However, the amount of drug that can be coated by this approach was not clinically significant. Hence, the stent metal surfaces have been modified to load a clinically relevant amount of drug ($\sim 100 \mu\text{g}/\text{cm}^2$) and to release it for a period of time. Nanoporous surfaces have been created on a 316 L SS stent surface by first coating it with a thin layer of aluminum by physical vapor deposition followed by anodization to convert aluminum to a porous aluminum oxide.¹⁶ However, particle debris liberated from this approach caused serious adverse reactions in animal studies.¹⁷ Carbon–carbon coatings,¹⁸ nanoporous metals,¹⁹ and porous calcium phosphate coatings²⁰ have also been used to deliver drugs directly from 316 L SS stent surfaces. A microrough surface of 316 L SS stents has been created by grit blasting and is used to deliver rapamycin (sirolimus).²¹ Although the clinical performance of this stent is encouraging,²² no reports are available on the detailed preparation or characterization of these surfaces. Also, most of these polymer-free drug delivery approaches have been carried out on 316 L SS. Co–Cr alloys are the current metal of choice for making stents due to their ability to make thinner struts with superior mechanical properties. Recently, the U.S. Food and Drug Administration (FDA) has approved two Co–Cr alloy stents, Endeavor and Xience V, for commercial use.²³

A variety of drugs have been delivered from stents. However, the two drugs that are most commonly used are paclitaxel (PAT) and sirolimus. The unique advantage of PAT is its strong adhesion property toward a variety of material surfaces.^{24–26} We previously demonstrated the use of such natural adhesion property of PAT to coat it directly on flat Co–Cr alloy surfaces.²⁶ However, the amount of drug that can be sustained released was in nanograms. If the amount of drug loading was increased to micrograms, most of the drug was released on the first day (burst effect). In order to be a clinically effective approach, the amount of drug has to be sustained released in micrograms for at least 2 weeks. We also demonstrated the use of self-assembled monolayers (SAMs) on flat Co–Cr alloy surfaces to increase the affinity of PAT toward alloy surfaces, thereby slowing the drug release.²⁷

The main goal of this study is to deliver PAT from microrough Co–Cr alloy surfaces. A significant advantage of using microrough surfaces over flat surfaces is that, once the drug is released, the underlying microrough topography can greatly favor the growth of endothelial cells,^{28–30} which can prevent late stent thrombosis.^{31,32} However, the rough surfaces can also promote the adhesion of blood platelets and cause thrombosis.^{33,34} It has been shown in the literature that the surfaces carrying negatively charged functional groups significantly reduce the thrombosis on mechanically rough surfaces³⁵ and several other material surfaces.^{36–38} Hence, we coated the microrough Co–Cr alloy surfaces with SAMs carrying –COOH terminal groups (provides negative surface charge as $-\text{COO}^-$ at physiological pH 7.4) and investigated the delivery of PAT from these surfaces as well.

To the best of our knowledge, no prior studies have been carried out on the following: (a) delivery of PAT from bare microrough Co–Cr alloy surfaces; (b) investigating the effect

of different microrough Co–Cr alloy surface topographies on the coating and release of PAT; (c) the effect of SAMs on delivering PAT from microrough surfaces. These are the specific objectives of this study.

2. MATERIALS AND METHODS

2.1. Materials. Ethanol (200 proof), acetone, methanol, 16-phosphonohexadecanoic acid (16-PHDA), and phosphate-buffered saline with 0.05 wt % tween-20 (PBS/T-20) were purchased from Sigma-Aldrich (USA). HPLC-grade water and acetonitrile were also purchased from Sigma-Aldrich (USA). Anhydrous tetrahydrofuran (THF) was purchased from Alfa Aesar (USA). Paclitaxel was purchased from ChemieTek (Indianapolis, IN). All chemicals were used as-received. High purity nitrogen (N_2) gas cylinders were purchased from Linweld (Lincoln, NE). Glass beads (Rolloblast 50 and 100 μm) and alumina (Cobra 50 and 110 μm) abrasive powders for grit blasting were purchased from Renfert USA Inc. (St. Charles, IL). Cobalt–chromium (Co–Cr) alloy (HAYNES 25 alloy) was purchased from Haynes International (Kokomo, IA).

2.2. Preparation of Microrough Co–Cr Alloy Specimens. The microrough specimens were prepared by grit blasting³⁹ (Basic Quattro, Renfert USA Inc. St. Charles, IL) the Co–Cr alloy plates (1 cm \times 1 cm) with the following four different kinds of abrasive powders: glass beads (50 μm in diameter), glass beads (100 μm), alumina (Al_2O_3) (50 μm), and Al_2O_3 (110 μm). The grit blasting was carried out at a gas (N_2) pressure of 60 psi for 1 min. The distance between the grit blasting nozzle and the sample surface was kept at a distance of 2 cm. Thus prepared microrough specimens were chemically cleaned by sonicating in ethanol, acetone, and methanol twice for 10 min each, followed by N_2 gas drying.²⁶ The microrough Co–Cr alloy specimens prepared by grit blasting with glass beads (50 μm), glass beads (100 μm), Al_2O_3 (50 μm), and Al_2O_3 (110 μm) are referred to here as Glass(50), Glass(100), Al_2O_3 (50), and Al_2O_3 (100), respectively. The abbreviations used for different samples used in this study are provided in Table 1.

Table 1. Abbreviations of Different Samples Used in the Study and Their Descriptions

abbreviations	explanations
Glass(50)	Co–Cr alloy grit blasted with glass (50 μm) beads
Glass(100)	Co–Cr alloy grit blasted with glass (100 μm) beads
Al_2O_3 (50)	Co–Cr alloy grit blasted with Al_2O_3 (50 μm) powder
Al_2O_3 (110)	Co–Cr alloy grit blasted with Al_2O_3 (110 μm) powder
Glass(50)-PAT	Co–Cr alloy grit blasted with glass (50 μm) beads and coated with PAT
Glass(100)-PAT	Co–Cr alloy grit blasted with glass (100 μm) beads and coated with PAT
Al_2O_3 (50)-PAT	Co–Cr alloy grit blasted with Al_2O_3 (50 μm) beads and coated with PAT
Al_2O_3 (110)-PAT	Co–Cr alloy grit blasted with Al_2O_3 (110 μm) beads and coated with PAT
Glass(50)-SAMs	Co–Cr alloy grit blasted with glass (50 μm) beads and coated with SAMs
Glass(100)-SAMs	Co–Cr alloy grit blasted with glass (100 μm) beads and coated with SAMs
Al_2O_3 (50)-SAMs	Co–Cr alloy grit blasted with Al_2O_3 (50 μm) beads and coated with SAMs
Al_2O_3 (110)-SAMs	Co–Cr alloy grit blasted with Al_2O_3 (110 μm) beads and coated with SAMs
Glass(50)-SAMs-PAT	Co–Cr alloy grit blasted with glass (50 μm) beads and coated with SAMs followed by PAT deposition
Glass(100)-SAMs-PAT	Co–Cr alloy grit blasted with glass (100 μm) beads and coated with SAMs followed by PAT deposition
Al_2O_3 (50)-SAMs-PAT	Co–Cr alloy grit blasted with Al_2O_3 (50 μm) beads and coated with SAMs followed by PAT deposition
Al_2O_3 (110)-SAMs-PAT	Co–Cr alloy grit blasted with Al_2O_3 (110 μm) beads and coated with SAMs followed by PAT deposition

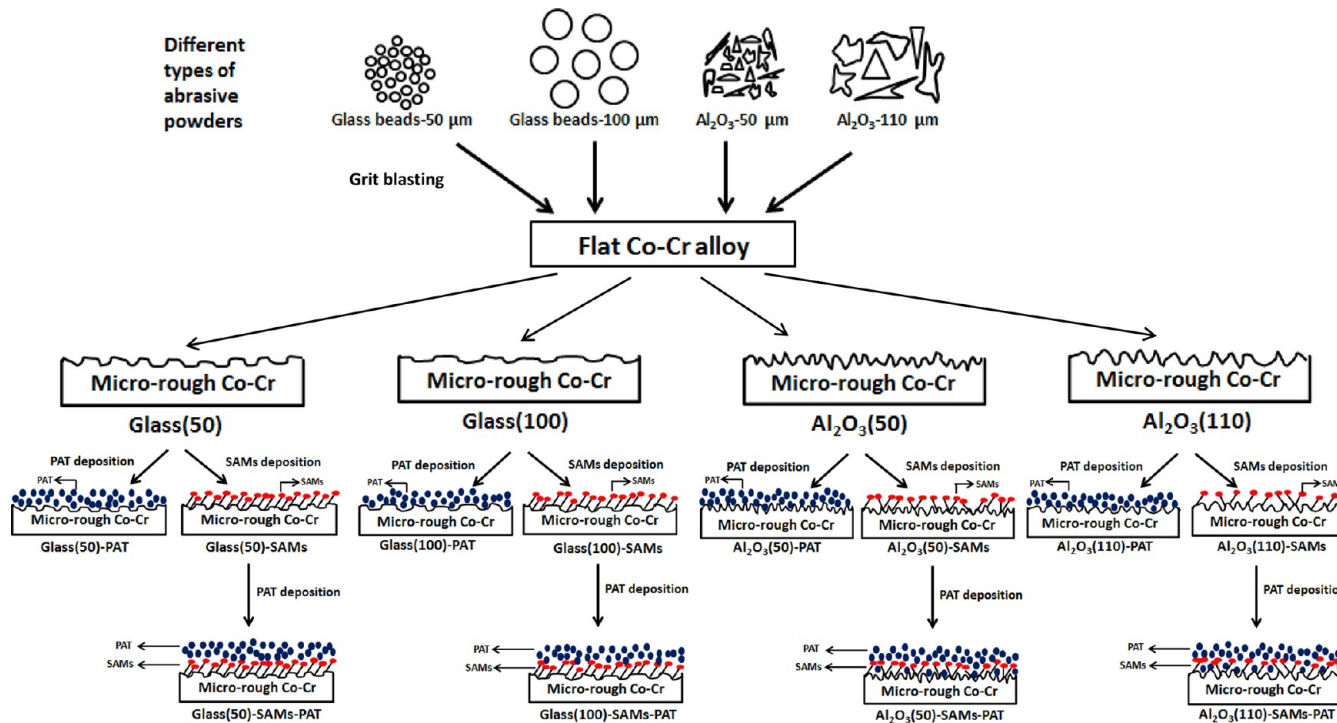


Figure 1. Schematic of preparation of PAT deposited bare microrough and SAM coated microrough Co-Cr alloy specimens.

2.3. Preparation of SAM Coated Microrough Co–Cr Alloy Specimens. Phosphonic acid SAMs were coated on microrough Co–Cr alloy specimens using a previously described procedure.²⁷ Briefly, the chemically cleaned microrough specimens were immersed in 3 mL of 1 mM solution of 16-PHDA in THF for 18 h. The samples were then transferred to an oven without rinsing and heat treated at 120 °C for 18 h. After heat treatment, the specimens were cleaned by sonication in THF and deionized water (di-H₂O) for 1 min each followed by N₂ gas drying. The microrough Co–Cr alloy specimens prepared by grit blasting with glass beads (50 μm), glass beads (100 μm), Al₂O₃ (50 μm), and Al₂O₃ (110 μm) and coated with SAMs are referred to here as Glass(50)-SAMs, Glass(100)-SAMs, Al₂O₃(50)-SAMs, and Al₂O₃(110)-SAMs, respectively (Table 1).

2.4. Deposition of Paclitaxel on Microrough Co–Cr Alloy Specimens. Paclitaxel (PAT) was coated on bare microrough (without SAM coating) and SAM coated microrough specimens by the microdrop deposition method as previously demonstrated.²⁶ Briefly, a solution of paclitaxel in ethanol was prepared at a concentration of 4 mg/mL. A 25 μL aliquot of the prepared PAT solution was carefully placed on the specimens. The ethanol was allowed to evaporate for 3 h, leaving a thin film of PAT on microrough specimens. The total amount of drug loaded on microrough Co–Cr alloy specimens was 100 μg/cm². PAT coated glass(50), glass(100), Al₂O₃(50), and Al₂O₃(110) specimens are referred to here as Glass(50)-PAT, Glass(100)-PAT, Al₂O₃(50)-PAT, and Al₂O₃(100)-PAT, respectively (Table 1). PAT coated Glass(50)-SAMs, Glass(100)-SAMs, Al₂O₃(50)-SAMs, and Al₂O₃(110)-SAMs are referred to here as Glass(50)-SAMs-PAT, Glass(100)-SAMs-PAT, Al₂O₃(50)-SAMs-PAT, and Al₂O₃(110)-SAMs-PAT, respectively (Table 1). The schematic of preparation of PAT coated microrough specimens is provided in Figure 1.

2.5. Surface Characterization. The different specimens prepared in this study including bare microrough, SAM coated microrough, and PAT deposited bare and SAM coated microrough were characterized using scanning electron microscopy, optical profilometry, and Fourier transform infrared spectroscopy.

2.5.1. Scanning Electron Microscopy (SEM). The surface morphology of the specimens was observed by scanning electron microscope (Model No. Quanta 450, FEI, USA). An accelerating voltage of 30.00 kV was used during the SEM imaging. The images

were captured at 1000× magnification. The specimens were sputter coated with 20 nm thickness of gold–palladium coating prior to SEM imaging to prevent surface charging by the electron beam.

2.5.2. Optical Profilometry. The specimens were characterized using a Wyko NT8000 optical surface profilometer (operated at Michigan Metrology LLC) to obtain three-dimensional (3D) topography, roughness, surface area, normalized surface volume, and surface slope measurements. The different parameters that were employed in the optical profilometer characterization of microrough specimens are provided in Table 2. The roughness, surface area,

Table 2. The Primary Parameters of 3D Optical Profilometry Used for Measurement and Analysis

measurement attribute	nominal value
magnification	10.2×
measurement array size	640 × 480
lateral sampling	0.97 μm
field of view	623 μm × 467 μm
3D filter	Gaussian – long wave pass short wavelength cutoff = 0.006 mm
height resolution	<6 nm
bearing ratio offsets peak/valley	1%/1%
Stylus X λc/λs	0.60 mm/6 μm
Stylus X λc/λs	0.45 mm/4.5 μm
Stylus filter type	Gaussian

normalized surface volume, and surface slope values reported here represent the average of three distinct spots on a sample along with the corresponding standard deviation.

2.5.3. Fourier Transform Infrared (FTIR) Spectroscopy. A Nicolet 6700 FTIR (Thermo Scientific) spectrometer equipped with a Smart SAGA (Specular Aperture Grazing Angle) accessory was used to characterize the SAMs and PAT coatings on microrough specimens. The IR spectra were collected at an average angle of 80° relative to the surface normal. A germanium polarizer mounted in the accessory minimizes the “S” polarized light and provides increased sensitivity. For each spectrum, 32 scans were collected at a resolution of 4 cm⁻¹.

The collected spectra were baseline corrected and analyzed using OMNIC software.

2.6. Drug Elution Studies. All PAT deposited bare and SAM coated microrough Co–Cr alloy specimens ($n = 4$ for each group) were immersed in 20 mL of PBS/T-20 solution (pH 7.4) and incubated at 37 °C in a circulating water bath (Precision, model no. 2866, Thermo Scientific, USA). Tween-20, a nonionic surfactant, is commonly added to increase the solubility of PAT in PBS and to maintain sink conditions.^{40–43} At predetermined time intervals, the alloy specimens were taken out of the solution and transferred to fresh PBS/T-20 solution. The PBS/T-20 samples collected every day for up to 14 days were analyzed for the amount of drug released using high performance liquid chromatography (HPLC). As recommended previously,²⁶ 1 mL of ethanol was added to the PBS/T-20 solution prior to HPLC analysis to remove PAT physically adsorbed onto the polypropylene containers used in drug-elution studies.

2.6.1. High Performance Liquid Chromatography. A reverse-phase HPLC (Waters e2695 separations module with Waters 2489 UV/visible detector) was used to quantify the amount of PAT released. The HPLC protocols for quantifying the PAT released were carried out as described previously.²⁶ Briefly, a mobile phase of water and acetonitrile (45:55, v/v) was used at a flow rate of 1 mL/min. A 10 μL aliquot of the sample was injected for analysis using a Nova-Pak C18 4 μm column (WAT086344). The UV–vis detector was set at 227 nm. A correlation coefficient of $R^2 = 0.99$ was obtained with a linear plot for the samples used for calibration in the concentration range of 1 ng/mL to 100 $\mu\text{g}/\text{mL}$. The Waters Millennium 32 software system was used to analyze the collected HPLC data.

2.7. Drug Extraction from the Microrough Co–Cr Alloy Surfaces after Drug Elution Studies. This experiment was carried out to determine the amount of PAT retained on the alloy samples after drug release studies. After 14 days of drug elution, all the alloy samples were transferred to 2 mL of ethanol (solvent for PAT) and sonicated for 10 min thrice with fresh solvent each time. Finally, the samples were sonicated in 2 mL of deionized water (di-H₂O) for 10 min. All the solutions (three ethanol samples and one di-H₂O sample) collected were used in HPLC to determine the amount of PAT extracted from the alloy samples.

2.8. Statistical Analysis. The experimental data collected are provided as mean \pm standard deviation. A one-way analysis of variance (ANOVA) was carried out, and the statistical significance for difference was defined as $p < 0.05$.

3. RESULTS

3.1. SEM Characterization. Figure 2A shows the SEM image of as-received Co–Cr alloy prior to grit blasting. The surfaces were flat with few surface defects such as scratches and shallow grooves arisen from the metal processing. Figure 3A–D shows the SEM images of Glass(50), Glass(100), Al₂O₃(50), and Al₂O₃(110), respectively. These images showed the successful formation of microrough Co–Cr alloy surfaces. The glass beads produced the least amount of blasting scars (Figure 3A and B), while the Al₂O₃ produced the greatest amount of blasting scars (Figure 3C and D) on the alloy surface. The visual inspection of SEM images showed that the amount of scars produced by grit blasting increased in the following order: Glass(50) < Glass(100) < Al₂O₃(50) = Al₂O₃(100). Figure 3E–H shows the SEM images of microrough Co–Cr alloy surfaces after PAT coating. The deposition of PAT was evident from the SEM images, as the scars of microrough surfaces were uniformly covered by PAT. Figure 4 shows the SEM images of SAM coated microrough Co–Cr alloy surfaces without and with PAT coating. No significant difference in the surface morphology was observed between SAM coated microrough surfaces (Figure 4A–D) and bare microrough surfaces (Figure 3A–D). Similar to Figure

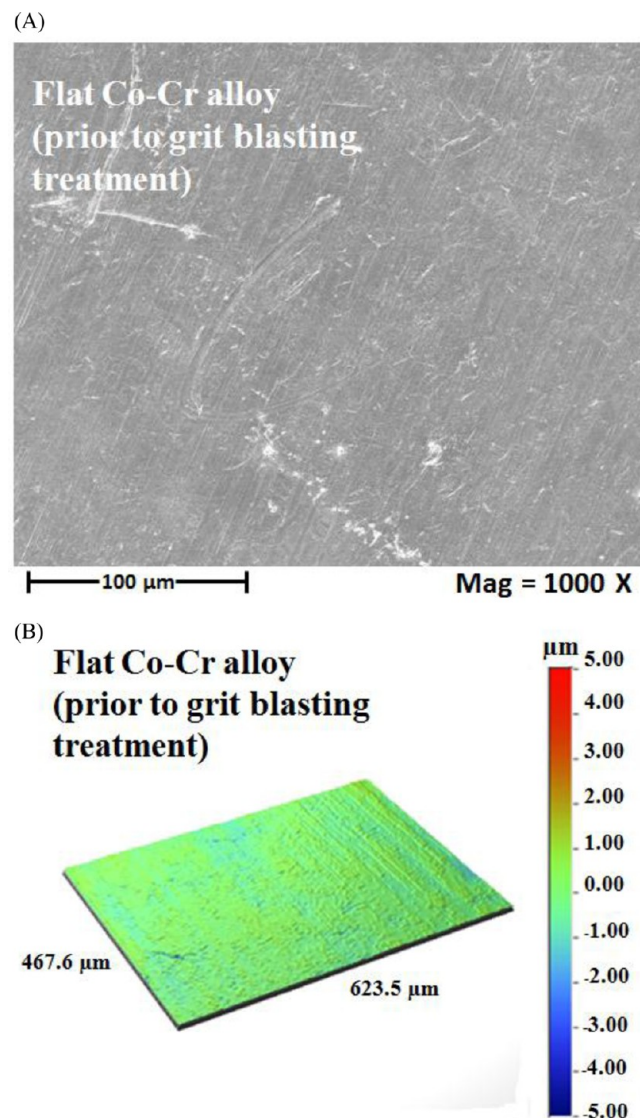


Figure 2. SEM (A) and optical profilometry (B) images of flat Co–Cr alloy surface prior to grit blasting treatment.

3E–H, the scars of SAM coated microrough surfaces were uniformly covered by PAT coating (Figure 4E–H).

3.2. 3D Optical Profilometry Characterization. Figure 2B shows the 3D optical profilometry topography image of as-received Co–Cr alloy. In agreement with the SEM data, these images showed a flat surface with few surface defects. Figures 5 and 6 show the 3D optical profilometry topography images (467.6 $\mu\text{m} \times 623.5 \mu\text{m}$) of bare and SAM coated microrough Co–Cr alloy surfaces without and with PAT coating, respectively. These images clearly showed the formation of different microrough topographies depending on the nature of the abrasive powders used (glass vs alumina) and the size of the powders (50 μm vs 100 μm) (Figure 5A–D). The deposition of PAT on the microrough surfaces is also evident from these images (Figure 5E–H). Similar results were observed for the SAM coated microrough specimens without (Figure 6A–D) and with PAT coating (Figure 6E–H).

The roughness (S_a) values of all the different surfaces used in this study were determined using optical profilometry for a scan size of 467.6 $\mu\text{m} \times 623.5 \mu\text{m}$ and are provided in Table 3. S_a is defined as the average roughness evaluated over the complete

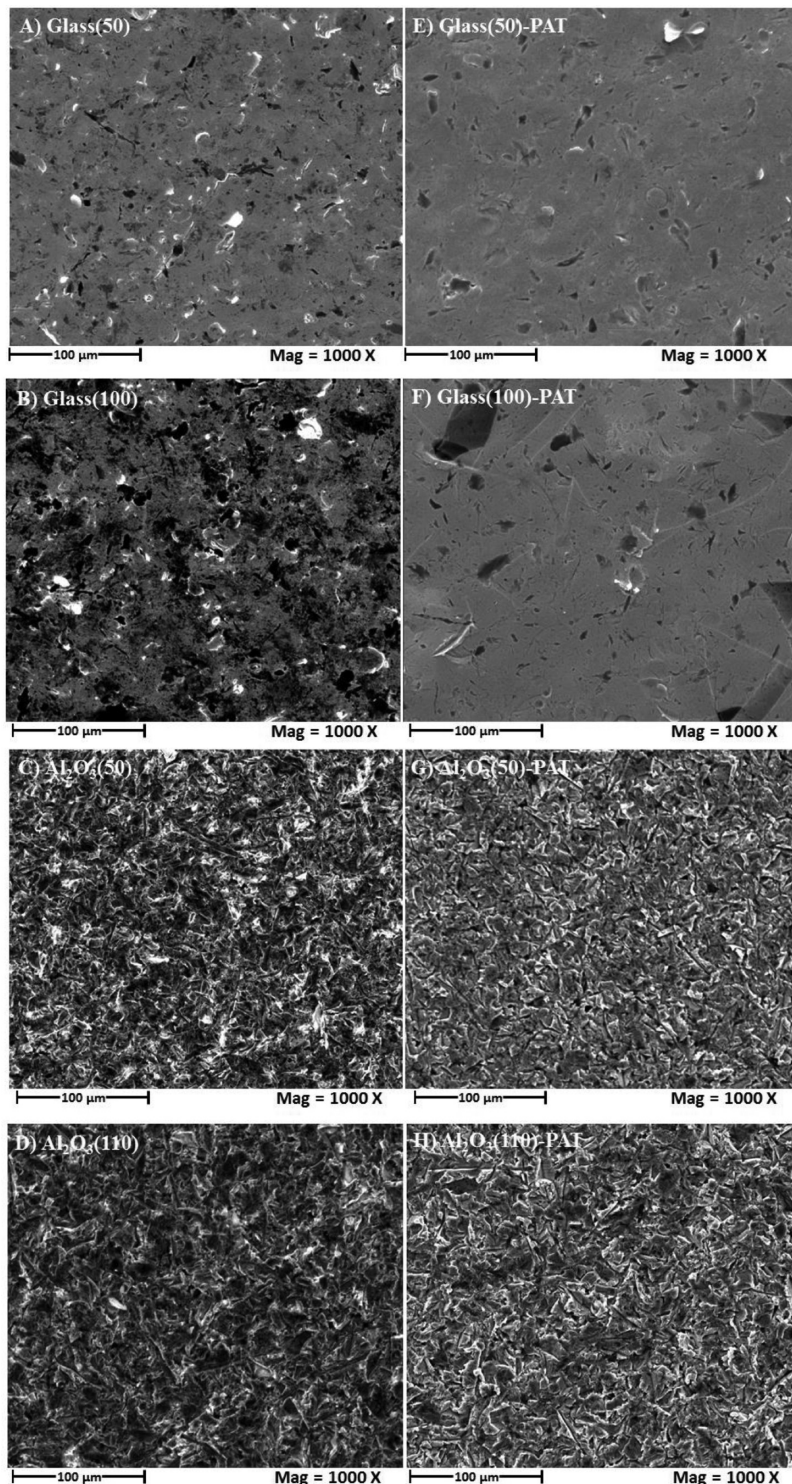


Figure 3. SEM images of bare microrough Co–Cr alloy surfaces without (left column) and with PAT coating (right column).

3D surface. The Ra value of flat Co–Cr alloy was measured as $0.26 \pm 0.02 \mu\text{m}$. The Ra values of all the microrough surfaces were significantly ($p < 0.05$) greater than that of the flat Co–Cr alloy surface (Table 3). The increasing order of roughness for bare microrough surfaces was determined as follows: $\text{Al}_2\text{O}_3(100) < \text{Al}_2\text{O}_3(50) = \text{Glass}(50) < \text{Glass}(100)$. Although SEM images showed a greater number of scars for Al_2O_3 grit blasted surfaces than glass bead grit blasted surfaces, it is interesting to observe that the roughness of glass bead grit

blasted surfaces was actually greater than that of Al_2O_3 grit blasted surfaces for the scan area ($467.6 \mu\text{m} \times 623.5 \mu\text{m}$) measured in this study. This suggests that the visual appearance of the number of scars shown by SEM images should not be considered for estimating its surface roughness. After PAT coating, the Ra value of Glass(50) increased, while the Ra values of Glass(100) and $\text{Al}_2\text{O}_3(50)$ decreased when compared to their respective surfaces before drug coating. No significant difference in Ra values was observed for $\text{Al}_2\text{O}_3(110)$ surfaces

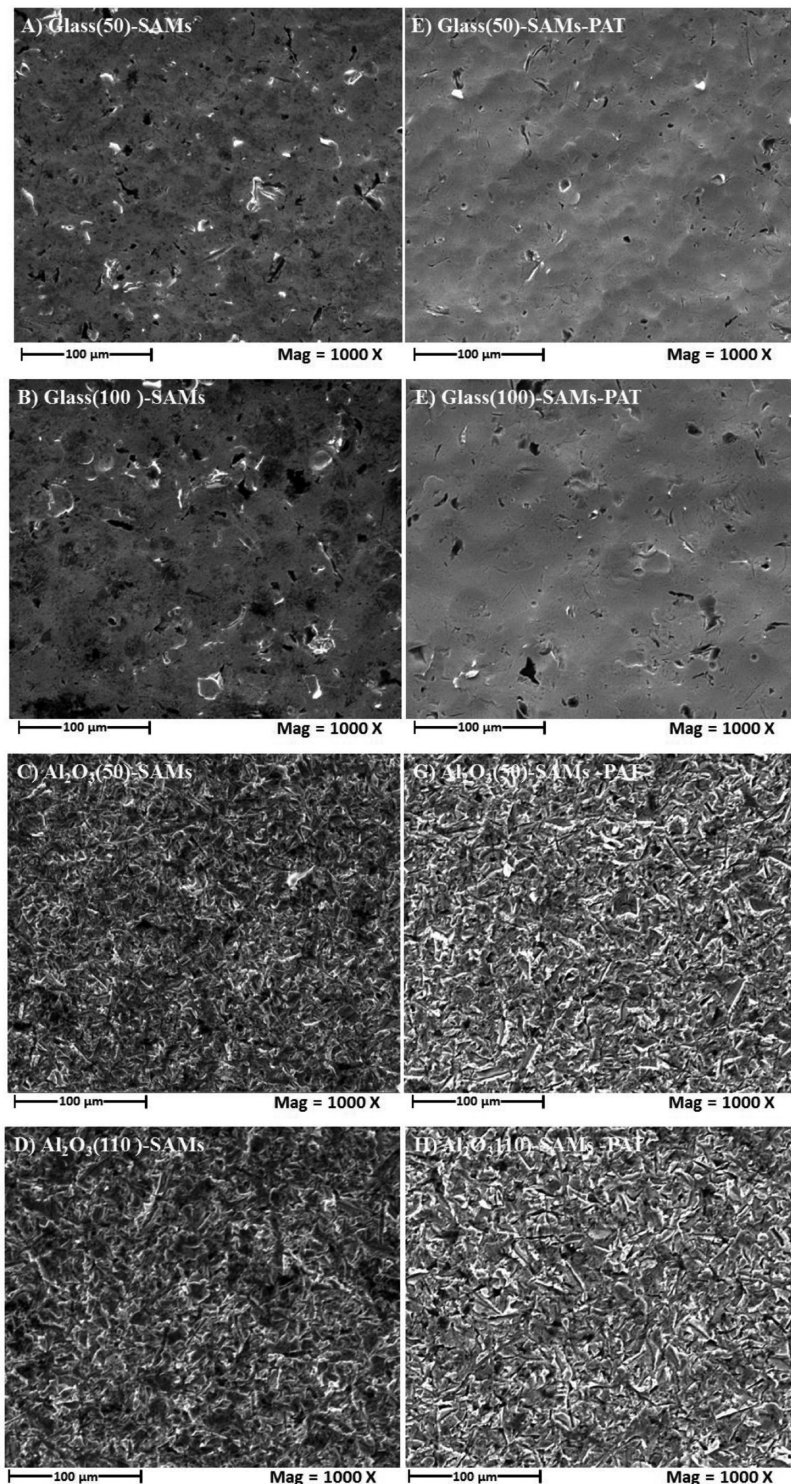


Figure 4. SEM images of SAM coated microrough Co–Cr alloy surfaces without (left column) and with PAT coating (right column).

before and after PAT coating. These results suggest that the surface roughness is altered by the way that the PAT is actually deposited on different topographies.

The Ra values of SAM coated microrough surfaces are provided in Table 3. In the literature, when the SAMs were coated on metal surfaces, the difference in the surface roughness values observed before and after SAM deposition was used as an indicator for studying the orderliness of the monolayer.^{44–46} No significant difference in the roughness values has been attributed to the formation of ordered films

which followed the underlying substrate topography, while a significant difference in the roughness values has been observed for disordered films with defects.^{44–46} In this study, no significant differences in the Ra values were observed for Glass(50) and Glass(100) surfaces before and after SAM deposition (Table 3). This suggests that the SAM coating was ordered and followed the contour of Co–Cr alloy surfaces grit blasted with glass beads irrespective of the bead size used. However, significant differences in the roughness values were observed for Al₂O₃(50) and Al₂O₃(110) surfaces before and

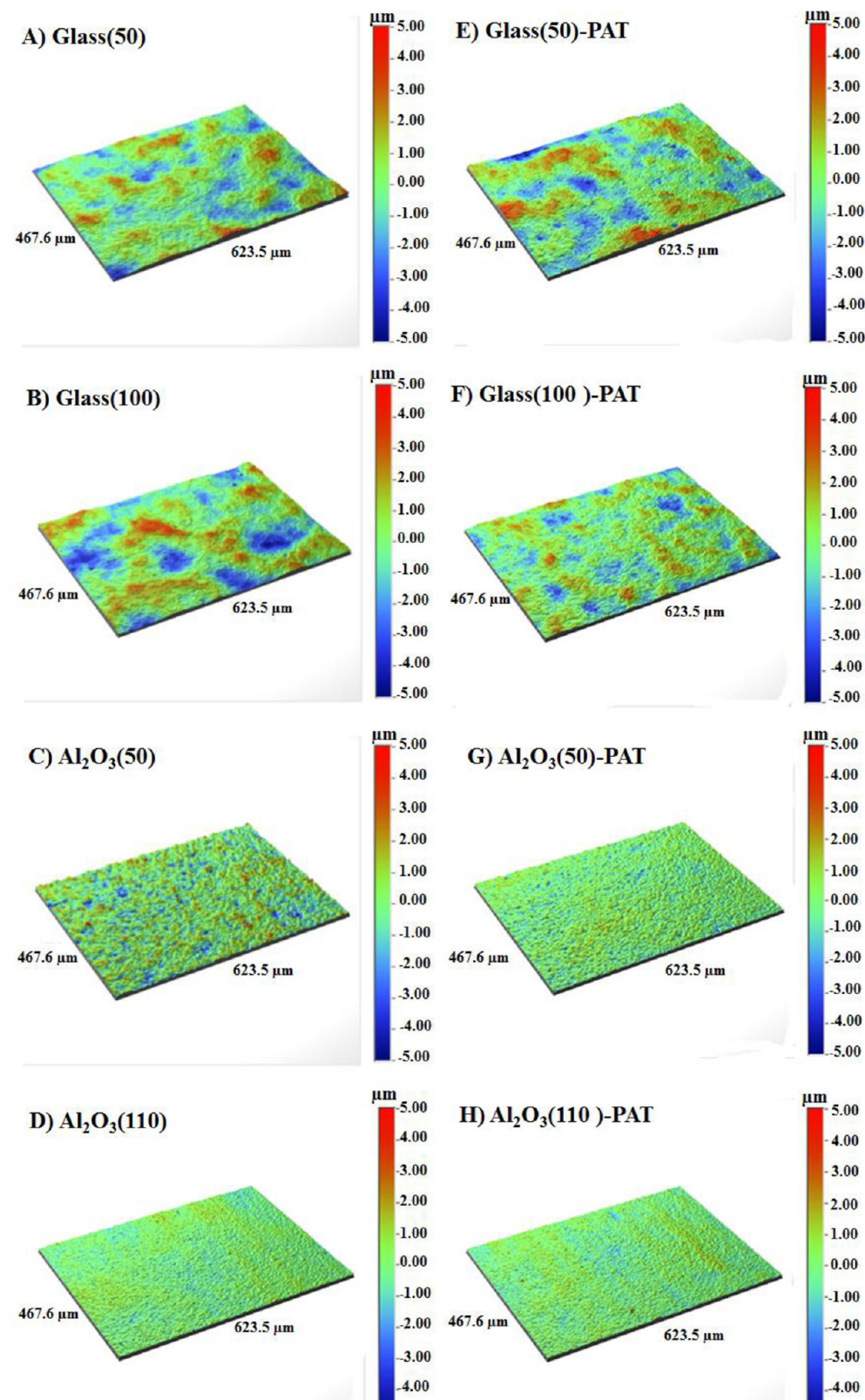


Figure 5. 3D optical profilometry images of bare microrough Co–Cr alloy surfaces without (left column) and with PAT coating (right column).

after SAM deposition (Table 3). The Ra value decreased from 0.8 ± 0.05 to 0.35 ± 0.01 μm for Al₂O₃(50) surfaces, while the value increased from 0.37 ± 0.02 to 0.45 ± 0.04 μm for Al₂O₃(110) surfaces. Such significant differences in the Ra values suggest that the monolayers were not ordered on Co–Cr

alloy surfaces grit blasted with Al₂O₃ powder. After PAT coating on SAM coated surfaces, no significant differences in the Ra values were observed for Glass(50), Glass(100), and Al₂O₃(110), while there is a slight increase observed for Al₂O₃(110).

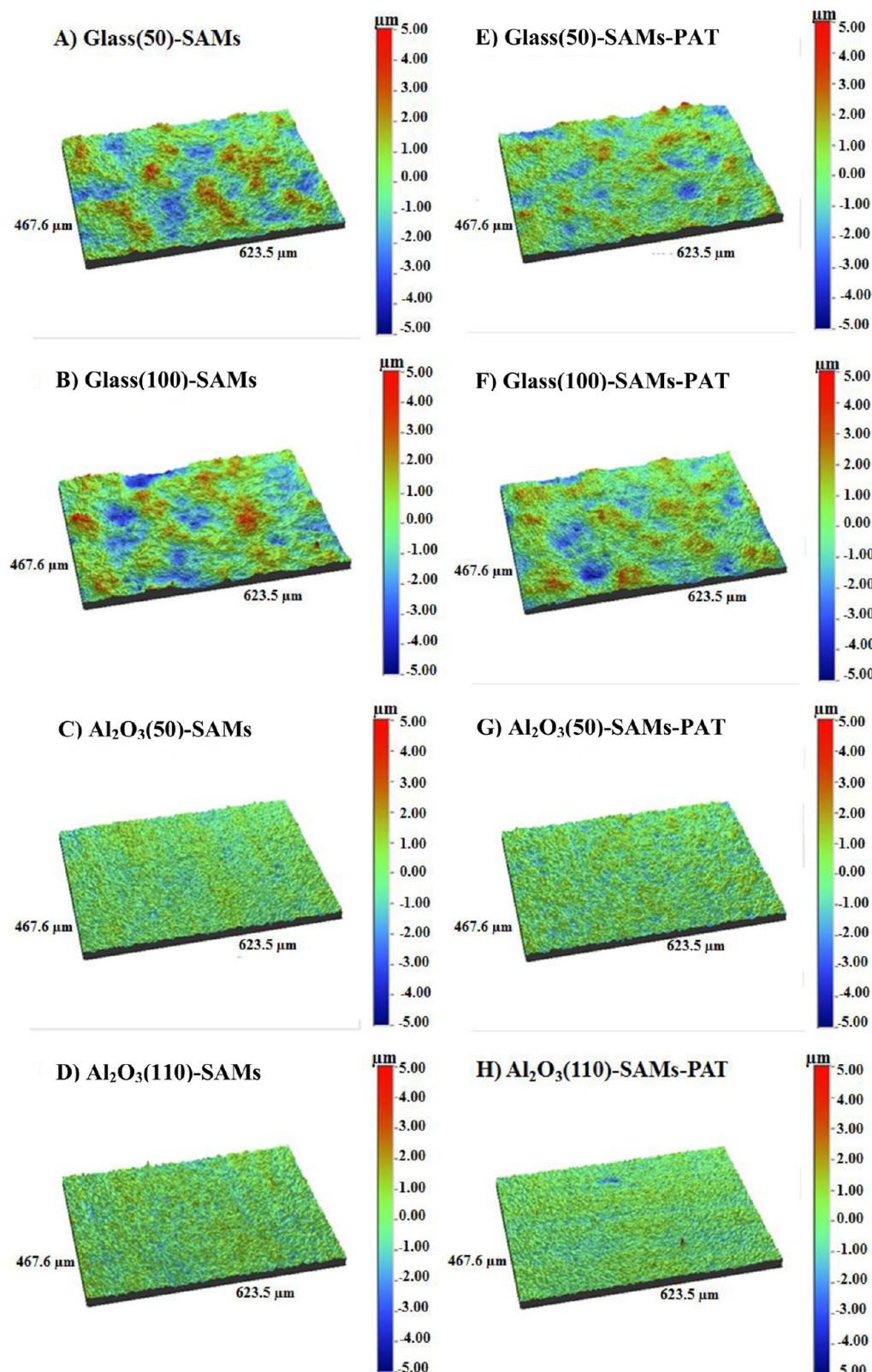


Figure 6. 3D optical profilometry images of SAM coated microrough Co–Cr alloy surfaces without (left column) and with PAT coating (right column).

The surface area (S_{dr}) of all the different surfaces used in this study was determined using optical profilometry and is provided in Table 3. S_{dr} is expressed as the percentage of additional surface area contributed by the texture as compared

to an ideal plane the size of the measurement region. The surface area of flat Co–Cr alloy was determined as $0.50 \pm 0.04\%$. The surface area obtained for microrough surfaces was significantly ($p < 0.05$) greater than that of flat Co–Cr alloy.

Table 3. The Average Roughness (Sa), the Surface Area (Sdr), the Normalized Surface Volume (NSVol), and the Surface Slope (Sdq) Determined by Optical Profilometry for Different Microrough Co–Cr Alloy Samples Used in the Study

samples	Sa (μm)	Sdr (%)	NSVol (BSM)	Sdq (deg)
Flat	0.26 \pm 0.02	0.50 \pm 0.04	0.4 \pm 0.03	5.7 \pm 0.2
Glass(50)	0.85 \pm 0.07	1.23 \pm 0.02	1.5 \pm 0.1	8.9 \pm 0.1
Glass(100)	1.10 \pm 0.12	1.17 \pm 0.07	2.1 \pm 0.2	8.8 \pm 0.3
Al_2O_3 (50)	0.80 \pm 0.05	7.23 \pm 0.72	1.3 \pm 0.1	21.3 \pm 1.0
Al_2O_3 (110)	0.37 \pm 0.02	2.08 \pm 0.28	0.6 \pm 0.1	11.6 \pm 0.8
Glass(50)-PAT	1.10 \pm 0.04	1.76 \pm 0.07	1.8 \pm 0.1	10.7 \pm 0.2
Glass(100)-PAT	0.83 \pm 0.06	1.59 \pm 0.09	1.3 \pm 0.1	10.2 \pm 0.3
Al_2O_3 (50)-PAT	0.49 \pm 0.05	3.28 \pm 0.46	0.8 \pm 0.1	14.5 \pm 1.0
Al_2O_3 (110)-PAT	0.41 \pm 0.04	2.71 \pm 0.56	1.2 \pm 0.7	13.2 \pm 1.4
Glass(50)-SAMs	0.86 \pm 0.08	1.4 \pm 0.1	1.6 \pm 0.1	9.7 \pm 0.3
Glass(100)-SAMs	1.01 \pm 0.05	1.4 \pm 0.02	1.8 \pm 0.3	9.4 \pm 0.1
Al_2O_3 (50)-SAMs	0.35 \pm 0.01	2.0 \pm 0.2	0.6 \pm 0.1	11.3 \pm 0.5
Al_2O_3 (110)-SAMs	0.45 \pm 0.04	3.4 \pm 0.5	0.7 \pm 0.1	14.7 \pm 1.0
Glass(50)-SAMs-PAT	0.85 \pm 0.11	1.38 \pm 0.05	1.5 \pm 0.1	9.5 \pm 0.2
Glass(100)-SAMs-PAT	0.97 \pm 0.13	1.86 \pm 0.27	1.6 \pm 0.2	11.0 \pm 0.8
Al_2O_3 (50)-SAMs-PAT	0.48 \pm 0.04	2.31 \pm 0.18	0.8 \pm 0.1	12.2 \pm 0.5
Al_2O_3 (110)-SAMs-PAT	0.39 \pm 0.04	2.18 \pm 0.22	0.8 \pm 0.2	11.9 \pm 0.6

The increasing order of the surface area of bare microrough surfaces is as follows: Glass(50) = Glass(100) < Al_2O_3 (100) \ll Al_2O_3 (50). After PAT coating, the Sdr of Al_2O_3 (50) significantly reduced from 7.23 ± 0.72 to $3.28 \pm 0.46\%$. This suggests that the majority of the cavities of Al_2O_3 (50) surfaces were filled by the drug. There is an increase in the surface areas of Glass(50) and Glass(100) after PAT coating. This suggests that the drug fills the cavities of Glass(50) and Glass(100) surfaces and forms a film with its own morphology. The surface area of such deposited PAT films was greater than that of its underlying alloy topography. The Sdr of Al_2O_3 (110) showed no significant differences before and after PAT coating. After SAM deposition, a slight increase in the Sdr was observed for Glass(50) (from 1.23 ± 0.02 to $1.4 \pm 0.1\%$) and Glass(100) (from 1.17 ± 0.07 to $1.4 \pm 0.02\%$) surfaces. However, a significant increase in Sdr was observed for Al_2O_3 (110) (from 2.08 ± 0.28 to $3.4 \pm 0.5\%$) surfaces, while a significant decrease in Sdr was observed for Al_2O_3 (50) (from 7.23 ± 0.72 to $2.0 \pm 0.2\%$) surfaces. In agreement with the surface roughness data, these results suggest the formation of ordered SAMs on glass grit blasted Co–Cr surfaces and disordered SAMs on alumina grit blasted Co–Cr surfaces. After PAT coating on SAM coated microrough surfaces, the Sdr value increased for Glass(100) and Al_2O_3 (50) surfaces, while it significantly decreased for the Al_2O_3 (110) surface and no change was observed for the Glass(50) surface. This suggests that the nature of PAT coating is different on SAM coated microrough surfaces when compared to bare microrough surfaces, since the change (increase or decrease or no change) in surface area after PAT

deposition is different for SAM coated vs bare microrough surfaces.

3.3. FTIR Characterization. The FTIR spectra of Glass(50)-PAT, Glass(100)-PAT, Al_2O_3 (50)-PAT, and Al_2O_3 (100)-PAT are provided in the Supporting Information # 1A–D, respectively. The strong IR absorbance bands for the C=O stretches of ester and amide functional groups in PAT were observed between 1730–1750 and 1630–1650 cm^{-1} , respectively. The peaks for the fingerprint regions of PAT were observed at 1250, 1070, and 717 cm^{-1} . These results showed the successful deposition of PAT on microrough Co–Cr alloy surfaces.

In the literature, the FTIR peaks for the symmetric and asymmetric stretches of –CH₂ groups in the alkyl chains of SAMs have been commonly used to confirm the presence of SAM on metal surfaces.^{47–49} Also, the peak positions of $\nu_{\text{symm}}(\text{CH}_2)$ and $\nu_{\text{asymm}}(\text{CH}_2)$ are used to study the order of alkyl chains in a SAM. For a well ordered SAM, the peak positions of $\nu_{\text{symm}}(\text{CH}_2)$ and $\nu_{\text{asymm}}(\text{CH}_2)$ have been observed at <2850 and $<2918 \text{ cm}^{-1}$, respectively.^{47–49} In our study, the $\nu_{\text{symm}}(\text{CH}_2)$ and $\nu_{\text{asymm}}(\text{CH}_2)$ peak positions of Glass(50)-SAMs and Glass(100)-SAMs were observed at 2912 and 2846 cm^{-1} and 2914 and 2848 cm^{-1} , respectively (Figure 7A,B). This suggested that the phosphonic acid molecules formed an ordered monolayer on Co–Cr alloy surfaces grit blasted with glass beads. The IR absorbance bands were negative for the Al_2O_3 (50)-SAMs and Al_2O_3 (110)-SAMs (Figure 7C,D). The negative peaks are attributed to the formation of disordered SAMs.⁴⁷ Also, the $\nu_{\text{symm}}(\text{CH}_2)$ and $\nu_{\text{asymm}}(\text{CH}_2)$ peak positions of Al_2O_3 (50)-SAMs and Al_2O_3 (100)-SAMs were observed at 2923 and 2853 cm^{-1} and 2917 and 2853 cm^{-1} , respectively (Figure 7C,D). These results suggested that the SAMs were not ordered on Co–Cr alloy surfaces grit blasted with Al_2O_3 abrasive powder. The FTIR data were in excellent agreement with optical profilometry data on the formation of ordered and disordered films on surfaces grit blasted with glass beads and Al_2O_3 , respectively.

The FTIR spectra of PAT on SAM coated microrough surfaces are provided in Supporting Information # 2. Similar to the results of PAT on bare microrough surfaces (Supporting Information # 1), the FTIR showed strong absorbance bands for the C=O stretches of ester and amide bonds and the fingerprint regions of PAT. These results showed the successful coating of PAT on SAM coated microrough Co–Cr alloy surfaces.

3.4. In Vitro Drug Release Studies. Figure 8a shows the cumulative PAT release profiles for bare microrough Co–Cr alloy surfaces. Glass(50)-PAT showed burst release as $30 \pm 1 \mu\text{g}$ of PAT was released on day-1 followed by a very slow release for up to 14 days ($38 \pm 2 \mu\text{g}$). When compared to Glass(50)-PAT, Glass(100)-PAT showed much reduced burst effect as only $11 \pm 2 \mu\text{g}$ of PAT was released on day-1 followed by $28 \pm 3 \mu\text{g}$ on day-2. After day-2, a very slow release of PAT was observed for up to 14 days ($36 \pm 2 \mu\text{g}$). Al_2O_3 (50)-PAT showed a sustained release profile as 8 ± 1 , 17 ± 4 , 28 ± 3 , and $33 \pm 2 \mu\text{g}$ of PAT were released on days-1, 2, 3, and 4, respectively. The release profile reached a plateau after 7 days, and the total amount of drug released after 14 days was $41 \pm 2 \mu\text{g}$. Similarly, Al_2O_3 (110)-PAT showed sustained release as 9 ± 1 , 16 ± 2 , 26 ± 3 , 34 ± 2 , 39 ± 2 , and $43 \pm 2 \mu\text{g}$ of PAT was released on days-1, 2, 3, 4, 5, and 6, respectively. The release profile reached a plateau after 7 days, and the total amount of drug released after 14 days was $48 \pm 2 \mu\text{g}$. Thus, these results

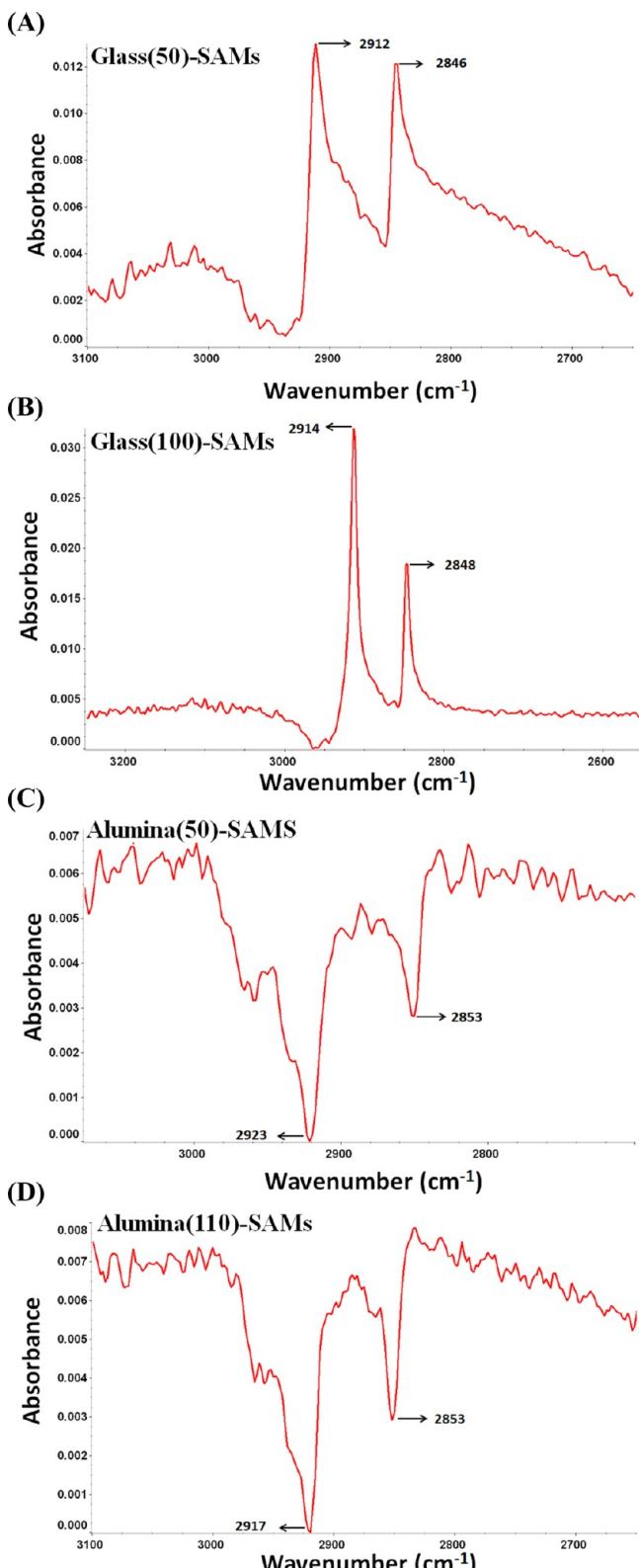


Figure 7. FTIR spectra of SAM coated microrough Co–Cr alloy specimens: Glass(50)-SAMs (A), Glass(100)-SAMs (B), Al_2O_3 (50)-SAMs (C), and Al_2O_3 (110)-SAMs(D).

demonstrated that bare microrough Co–Cr alloy surfaces prepared by grit blasting with glass-50 beads showed burst release, while the microrough surfaces prepared by glass-100 beads significantly reduced the burst effect. The microrough

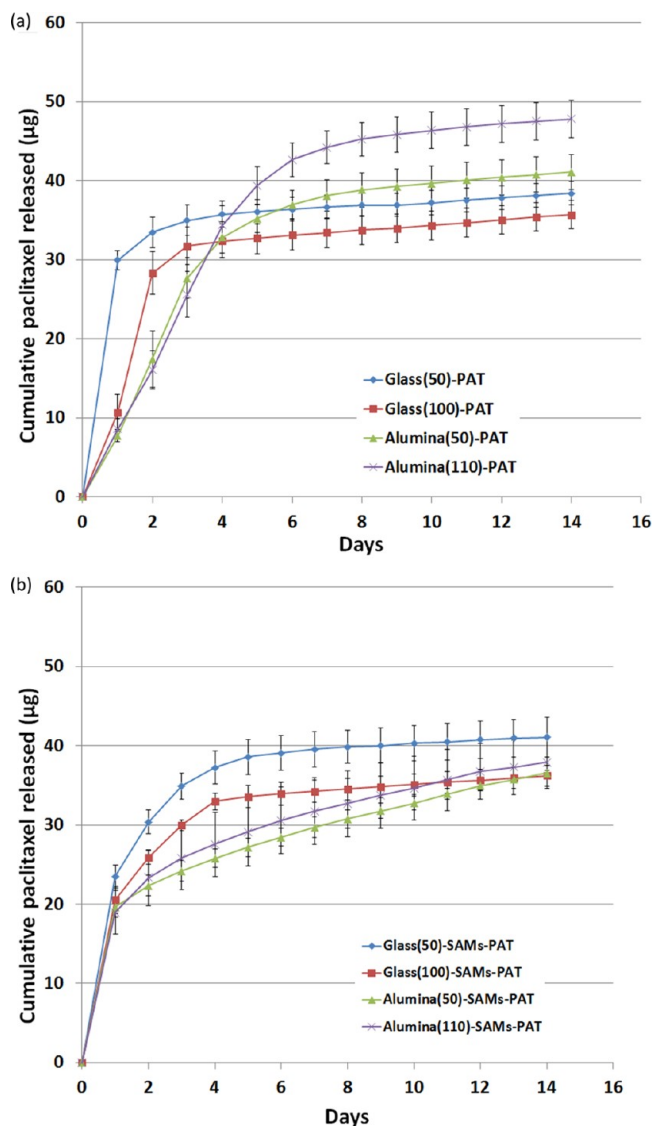


Figure 8. Cumulative paclitaxel release (μg) profiles of bare microrough Co–Cr alloy surfaces (a) and SAM coated microrough Co–Cr alloy surfaces (b).

surfaces prepared by Al_2O_3 powder showed sustained release profiles irrespective of the powder size employed in this study.

Figure 8b shows the cumulative PAT release profiles of SAM coated microrough Co–Cr alloy surfaces. All the SAM coated microrough surfaces showed biphasic release profiles; i.e., an initial burst was followed by a slow and sustained release for up to 14 days. For Glass(50)-SAMs-PAT, an initial burst of $23 \pm 1 \mu\text{g}$ on day-1 was followed by a sustained release of 30 ± 1 , 35 ± 2 , and $37 \pm 2 \mu\text{g}$ of PAT on days-2, 3, and 4, respectively. Similarly, for Glass(110)-SAMs-PAT, an initial burst of $21 \pm 2 \mu\text{g}$ on day-1 was followed by a sustained release of 26 ± 1 , 30 ± 1 , and $33 \pm 1 \mu\text{g}$ of PAT on days-2, 3, and 4, respectively. For both Glass(50)-SAMs-PAT and Glass(100)-SAMs-PAT, the release profiles reached a plateau after 4 days with the total amount of drug released after 14 days being 41 ± 2 and $36 \pm 1 \mu\text{g}$, respectively. The release profiles of Al_2O_3 (50)-SAMs-PAT and Al_2O_3 (110)-SAMs-PAT were very interesting. After an initial burst release of $\sim 20 \mu\text{g}$ on day-1, an amount close to $1 \mu\text{g}$ was sustained released on every day for up to 14 days. Figure 9 shows the amount of PAT released between every two

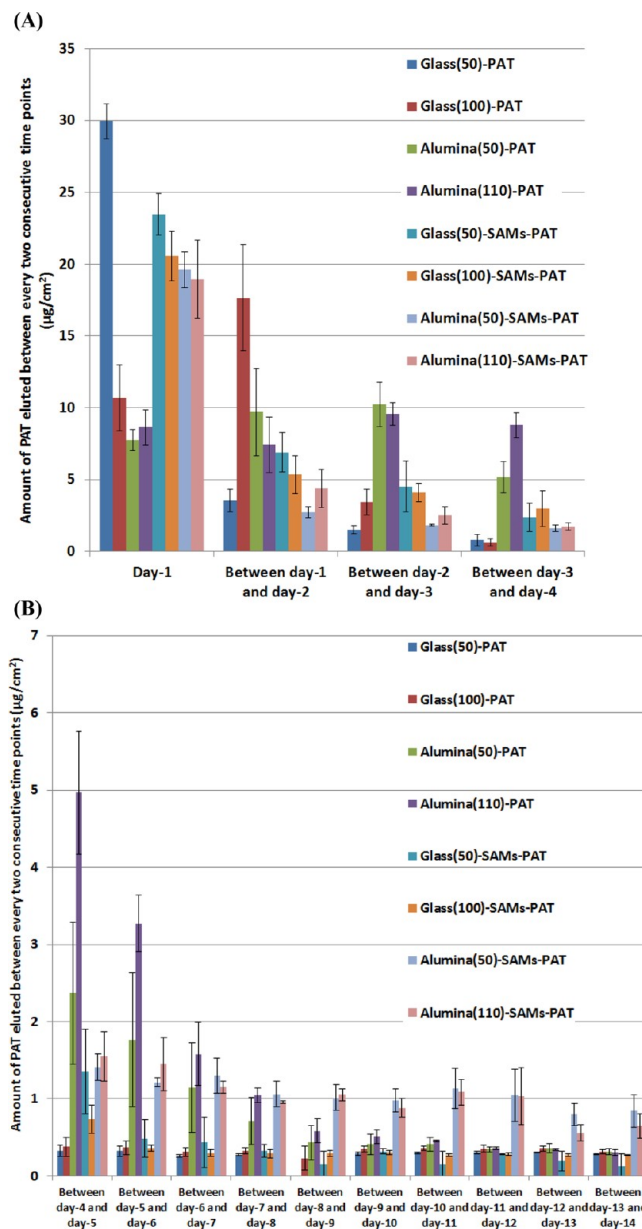


Figure 9. Amount of PAT eluted between every two consecutive time points of bare and SAM coated microrough Co–Cr alloy (A) from “day-1” to “between day-3 and day-4” and (B) from “between day-4 and day-5” to “between day-13 and day-14”.

consecutive time points for all eight different groups of specimens used in this study. The amount of drug eluted from $\text{Al}_2\text{O}_3(50)$ -SAMs-PAT and $\text{Al}_2\text{O}_3(110)$ -SAMs-PAT was significantly greater than that of other groups from day-8 to day-14, and consistent in releasing close to 1 $\mu\text{g}/\text{day}$ during the same time points. These results demonstrated the use of SAMs in prolonging the sustained release of a significant amount of PAT from microrough Co–Cr alloy surfaces.

3.5. Determination of the Amount of PAT Retained on Microrough Co–Cr Alloy Surfaces after 14 Days of Drug Elution Studies. Table 4 shows the amount of PAT extracted from the alloy samples after 14 days of drug elution. Most samples retained only 0.1–0.7 μg of PAT, while the $\text{Al}_2\text{O}_3(50)$ -SAMs-PAT and $\text{Al}_2\text{O}_3(100)$ -SAMs-PAT retained a slightly greater amount of PAT (9.65 ± 0.72 and 3.26 ± 2.47 , respectively) on the alloy surfaces.

4. DISCUSSION

The limitations of using polymers to deliver drugs from stents are as follows: (a) The drug containing polymers are typically coated on the stent in a crimped state. When the stent is expanded at the implantation site, the expanding stress may induce mechanical damage to the polymer coatings. A variety of irregularities including cracks, wrinkles, waviness, depressions, and peeling have been observed in some polymer coatings.^{50–53} Such irregularities may create adverse reactions in patients. (b) Some polymers induce chronic inflammatory and hypersensitivity reactions in patients.^{12,13,54–58} (c) The growth of endothelial cells on stents is vital for preventing late stent thrombosis (LST). Endothelial cells prevent LST by inhibiting the adhesion, aggregation, and activation of blood platelets. Polymer coatings may delay or inhibit the growth of endothelial cells on stents.^{11,13,14} This is considered to be one of the primary reasons for the occurrence of LST in polymer-coated DES.^{10–12} Hence, the polymer-free drug delivery platforms are promising for coronary stents.

In this study, the drug PAT was directly loaded on the microrough Co–Cr alloy surfaces generated by grit blasting and was delivered it for a period of two weeks without using polymer coatings. After the drug is delivered, the underlying microrough topography may favor endothelialization. The excellent growth of endothelial cells on microrough surfaces has been previously shown in the literature.^{28–30} However, rough surfaces have also been shown to promote the adhesion, aggregation, and activation of blood platelets and can cause thrombosis.^{33,34} In order to counteract this problem, rough surfaces with negative charges have been prepared.³⁵ Platelets have a net electronegative surface charge.³⁸ Hence, if the material also contains negative charge on its surface, the platelets would not adhere due to the repulsion between the two same charges.³⁸ Several studies in the literature have shown that the platelet adhesion was significantly reduced for the material surfaces carrying negatively charged functional groups such as $-\text{COOH}$ ³⁶ and $-\text{SO}_3\text{H}$.³⁷ Hence, microrough surfaces coated with SAMs carrying terminal $-\text{COOH}$ groups were also prepared and used for the drug delivery studies for potential applications in stents.

The generation of microrough Co–Cr alloy surfaces with different morphologies has been previously shown in the literature. Taga et al.³⁹ grit blasted the Co–Cr alloy surfaces with different types of abrasive powders including carborundum, Al_2O_3 , glass beads, and mixed powders comprising both Al_2O_3 and glass beads. SEM is commonly used to assess the roughness of grit blasted material surfaces. The lateral resolution of SEM is very good.⁵⁹ Hence, the finer spaced structures in Al_2O_3 grit blasted Co–Cr surfaces are clearly visible. Similarly, the wider spaced structures in glass bead grit blasted Co–Cr surfaces are also clearly seen. However, the depth resolution of SEM is not good because of the narrow aperture angles used.⁵⁹ Hence, the surfaces with finer spaced structures appear to be rough when compared to the surfaces with wider spaced structures. However, the measurement of volume of the cavities generated on the microrough surfaces would provide useful information regarding the nature of surface textures generated. Optical profilometry provides the normalized surface volume (NSVol), an important 3D surface parameter which measures the amount of fluid that would fill the surface from the lowest valley to the highest peak normalized to the measured cross sectional area. The unit for

Table 4. Total Amount of PAT Retained on the Microrough Co–Cr Alloy Surfaces after 14 Days of Drug Elution Studies

sample name	amount of PAT ($\mu\text{g}/\text{cm}^2$) extracted during the first 10 min sonication in ethanol	amount of PAT ($\mu\text{g}/\text{cm}^2$) extracted during the second 10 min sonication in ethanol	amount of PAT ($\mu\text{g}/\text{cm}^2$) extracted during the third 10 minute sonication in ethanol	amount of PAT ($\mu\text{g}/\text{cm}^2$) extracted during the 10 min sonication in di-H ₂ O	total amount of drug ($\mu\text{g}/\text{cm}^2$) extracted from the alloy surfaces (sum of the values in columns 2, 3, 4, and 5 of this table)
Glass(50)-PAT	0.06 ± 0.02	0	0	0	0.06 ± 0.02
Glass(100)-PAT	0.68 ± 0.60	0	0	0	0.68 ± 0.60
Al ₂ O ₃ (50)-PAT	0.73 ± 0.63	0	0	0	0.73 ± 0.63
Al ₂ O ₃ (110)-PAT	0.17 ± 0.09	0	0	0	0.17 ± 0.09
Glass(50)-SAMs-PAT	0.09 ± 0.08	0	0	0	0.09 ± 0.08
Glass(100)-SAMs-PAT	0.39 ± 0.67	0	0	0	0.39 ± 0.67
Al ₂ O ₃ (50)-SAMs-PAT	9.59 ± 0.72	0.06 ± 0.01	0	0	9.65 ± 0.72
Al ₂ O ₃ (110)-SAMs-PAT	3.23 ± 2.46	0.03 ± 0.01	0	0	3.26 ± 2.47

NSVol is billions of cubic micrometers per inch square (BCM). Table 3 shows the increasing order of NSVol of bare microrough surfaces is as follows: Al₂O₃(100) < Al₂O₃(50) = Glass(50) < Glass(100), which suggests that the volume of cavities produced during grit blasting was greatest for Glass(100) and smallest for Al₂O₃(100). This will influence the average distance between peaks and valleys of a surface texture (i.e., the average roughness). Hence, the roughness of glass bead (100 μm) grit blasted surfaces was found to be greater than that of Al₂O₃ grit blasted surfaces. As expected, the surface area was greater for the surfaces with finer spaced structures (Al₂O₃ grit blasted surfaces) when compared to that of wider spaced structures (glass bead grit blasted surfaces).

The formation of SAMs on rough metal surfaces has been previously investigated.^{60–63} The surface roughness of underlying metal substrate plays a crucial role in determining the orderliness of the SAMs. If the surface roughness of the metal is in the range of 1–10 nm, it creates defects in the SAMs formed and leads to its disorderliness. However, if the roughness is greater than 10 nm, it increases the coverage of SAMs without significantly affecting its orderliness.^{60–63} In this study, the formation of uniform and ordered SAMs on Glass(50) ($\text{Ra} = 0.85 \pm 0.07 \mu\text{m}$) and Glass(100) ($\text{Ra} = 1.10 \pm 0.12 \mu\text{m}$) was confirmed by both FTIR and optical profilometry. However, disordered SAMs were formed on Al₂O₃(50) and Al₂O₃(110), although the Ra values of these samples were 0.80 ± 0.05 and $0.37 \pm 0.02 \mu\text{m}$, respectively. This could be due to the reason that the finer spaced structures on Al₂O₃(50) or Al₂O₃(110) interfered with the formation of well-ordered SAMs. The surface parameter Sdq determined by optical profilometry provides the measurement of slopes of the surface texture. Sdq is mathematically defined as the room mean square (rms) of the surface slope within the sampling area. For a given average roughness, a wider spaced texture will have a lower Sdq value, while a finer spaced structure will have a greater Sdq value. Table 3 shows the increasing order of Sdq of bare microrough surfaces is as follows: Glass(50) = Glass(100) < Al₂O₃(100) ≪ Al₂O₃(50). This clearly suggests the presence of wider spaced textures on glass bead grit blasted surfaces and very finer spaced textures on Al₂O₃ grit blasted surfaces. Hence, the surface slope and the surface area of the underlying substrate are more important than surface roughness for determining the orderliness of SAMs.

PAT can form different morphologies including spherical,²⁶ needle,^{26,27} fibrous and elongated,⁶⁴ plate-like,⁶⁴ and powder-like²⁷ on flat metal surfaces. It is interesting to observe that no such morphologies were observed on the microrough surfaces. Instead, it forms a thin film-like coating after filling up the cavities on the microrough surfaces. We have previously investigated the release of PAT from flat Co–Cr alloy surfaces without²⁶ and with SAM coating.²⁷ When PAT is allowed to deposit on flat surfaces by the microdrop deposition method, it forms a molecular coating directly on the alloy surfaces followed by the deposition of its crystals on top of the molecular coating.²⁶ The Co–Cr alloy is enriched with surface hydroxyl (—OH) groups. Hence, the PAT forms extensive hydrogen bonding with the surface —OH groups to form the strongly bound molecular coating.²⁶ Also, the PAT makes intermolecular hydrogen bonding to form aggregates of crystals which are weakly bound to each other.²⁶ In drug release studies, the weakly bound PAT crystals are burst released while the strongly bound molecules are released at a sustained rate.²⁶ When the flat alloy surfaces have been coated with —COOH terminated phosphonic acid SAMs, the stability of PAT on the alloy surfaces was significantly increased due to the extensive hydrogen bonding interactions between the —OH functionalities (in —COOH groups) of SAMs and the —OH groups of PAT, the —NH groups of PAT, and the C=O functionalities of ester, ketone, and amide groups in PAT.²⁷ Biphasic release profiles (an initial burst followed by a sustained release) have been observed for the SAM coated alloy surfaces, while burst release profiles were observed for control alloy surfaces without SAM coating.²⁷

Microrough surfaces have increased surface area which provides more sites for the PAT to adsorb than that of flat surfaces. Co–Cr alloy surfaces grit blasted with Al₂O₃ showed much slower PAT release when compared to that of surfaces grit blasted with glass beads. This might suggest that the surfaces with greater surface area provide sustained release profiles. However, there are no significant differences in the amount of drug released between Al₂O₃(50) and Al₂O₃(110) at different time points, although the surface area was significantly different between these two surfaces (7.23 ± 0.72 vs $2.08 \pm 0.28\%$). Similarly, although there is no significant difference in the surface area observed between Glass(50) and Glass(110) (1.23 ± 0.02 vs $1.17 \pm 0.07\%$), the burst release on day-1 was

significantly reduced for Glass(100) when compared to that of Glass(50). These results suggest that surface area is not the sole parameter that influences the amount of drug release from microrough surfaces. The other parameters such as the surface features, the accessibility of available surface –OH groups to bond with PAT molecules, and the amount of PAT crystals formed may also play crucial roles in determining the amount of PAT released from various microrough Co–Cr alloy surfaces. The Al₂O₃(50)-SAMs-PAT and Al₂O₃(110)-SAMs-PAT prolonged the sustained release of a significant amount of PAT (~1 µg) throughout the second week (days-8 to 14) of drug elution studies (Figure 9B). All the other surfaces have showed the sustained release of a lesser amount of PAT (0.2 to 0.5 µg) during this time period. This might suggest that more PAT molecules were hydrogen bonded to the SAM coated Al₂O₃ grit blasted surfaces when compared to that of all the other surfaces. The absence of such behavior in Glass(50)-SAMs-PAT and Glass(100)-SAMs-PAT could be due to the presence of well-ordered and closed packed SAM on these surfaces in which the –COOH terminal groups have lesser access to PAT molecules for hydrogen bonding interactions due to the steric hindrance. However, in the case of Al₂O₃(50)-SAMs-PAT and Al₂O₃(110)-SAMs-PAT, the SAM is disordered; hence, the –COOH groups have greater access to PAT molecules for hydrogen bonding interactions due to the minimal steric hindrance.

From the results of drug extraction experiments (Table 4), it is clear that only a smaller amount of PAT was retained on the alloy surfaces after 14 days of drug elution studies. These results suggest that only 40–50 µg of PAT was released with a smaller amount of PAT retained on the alloy surfaces. These results are in agreement with several other studies in the literature reporting much lesser than 100% PAT release over a period of several weeks.^{65–70} Lee et al.⁶⁵ dip coated PAT directly on expanded polytetrafluoroethylene (ePTFE) grafts and investigated the drug release profile for up to 12 weeks. Only 50% of the total drug loaded was released from the grafts with the release profile getting saturated by the end of the period investigated in the study. Baek et al.⁶⁶ showed that only 40–50% of the total drug loaded was released from the ePTFE grafts for a period of 4 weeks. Several different release profiles (slow, moderate, and fast release) have been obtained for the commercially available PAT eluting TAXUS stent by varying the solvents used for the formulation and the drug-to-polymer ratio. All the release profiles showed the total amount of drug released in the range of <10 to ~60% over a period of few weeks.⁶⁷ Similar results of ~30 to ~60% of total PAT release were observed from the nanoparticles for cancer therapy applications.^{68–70} The two main reasons postulated in the literature for not observing 100% PAT release in most elution studies are (a) the binding of PAT to the walls of container surfaces^{24,71} and (b) the low stability of PAT in aqueous solutions.^{72,73} Song et al.²⁴ have shown that PAT bound to glass and various plastic container surfaces including polypropylene (PP). A greater amount of PAT was bound to glass than PP container surfaces. Although a methanol wash was able to recover some of the PAT adsorbed onto the container surfaces, not all of the bound PAT was removed. Similar results of drug adsorption to container surfaces have been observed in other studies for PAT⁷¹ and various other therapeutic drugs.⁷⁴ It was reported that the stability of PAT in aqueous solution is low, since the drug can undergo epimerization and hydrolysis.^{72,73} The C7 hydroxyl group in the chemical structure of

PAT is subjected to epimerization.⁷² Also, the PAT contains several hydrolytically sensitive ester groups. These ester groups have been shown to cleave by hydrolysis under neutral (pH 7) and basic (pH > 7) conditions in aqueous solutions.⁷³

The amount of PAT retained on most of the microrough Co–Cr alloy surfaces after 14 days of drug elution was determined as <1 µg/cm², while the amounts of 9.7 and 3.3 µg/cm² were retained on Al₂O₃(50)-SAMs-PAT and Al₂O₃(110)-SAMs-PAT, respectively (Table 4). The amount of residual PAT may have an effect on the potential endothelialization of stents. Jabara et al.⁷⁵ have shown that a low dose of PAT of 15 µg/cm² with a slower release rate did not affect the healing of the vessel wall as the implanted stents were endothelialized in a porcine study. In another study, the Stellium stent with a drug dose of 10.3 µg/cm² was implanted in human patients.⁷⁶ These stents showed promising results with no major adverse reactions. The Conor stent which carries 10 µg of PAT was found to be safe in human clinical trials.⁷⁷ Referencing this literature, in this study, since the amount of PAT retained is <1 µg/cm² in most of the microrough Co–Cr alloy surfaces (and <10 µg/cm² in SAM coated alumina grit blasted surfaces), it is expected that these surfaces would not adversely affect the endothelialization.

5. CONCLUSIONS

There is a need for polymer-free drug delivery platforms for the stent material such as Co–Cr alloy. In this study, eight different types of microrough Co–Cr alloy surfaces were prepared, characterized, and evaluated for the delivery of paclitaxel. Grit blasting using different beads (glass and Al₂O₃) and different sizes (50 and 100 µm) were used to create microrough Co–Cr alloy surfaces. The microrough surfaces were also surface modified using –COOH terminated SAMs to enhance the hydrogen bonding interactions between PAT and the alloy surfaces. SEM images were useful for distinguishing between the different surface morphologies generated and for observing changes in surface morphology after PAT coating. The optical profiler showed the 3D topography images of different surfaces, and the changes in surface roughness and surface area after the microrough specimens were coated with SAMs and PAT. In agreement with optical profiler data, the FTIR showed that the SAMs were ordered on glass bead grit blasted surfaces and the molecules were disordered on Al₂O₃ grit blasted surfaces. The successful deposition of PAT on all the different surfaces was confirmed by FTIR. Sustained PAT release profiles were observed for Al₂O₃ grit blasted bare microrough surfaces, while burst PAT release profiles were observed for glass bead grit blasted surfaces. All SAM coated surfaces showed biphasic release profiles which is an initial burst release followed by a slow and sustained release. The sustained release of PAT in significant amount was prolonged in SAM coated Al₂O₃ grit blasted surfaces, while this behavior was not present in any of the other surfaces used in this study. Thus, this study successfully showed the use of different microrough Co–Cr alloy surfaces for delivering paclitaxel without polymer coatings for potential applications in cardiovascular stents and other medical devices.

■ ASSOCIATED CONTENT

Supporting Information

FTIR spectra of paclitaxel deposited bare and SAM coated microrough Co–Cr alloy specimens. This material is available free of charge via the Internet at <http://pubs.acs.org>.

AUTHOR INFORMATION

Corresponding Author

*E-mail: Gopinath.Mani@usd.edu.

Notes

The authors declare no competing financial interest.

ACKNOWLEDGMENTS

This study was supported by a National Scientist Development Grant Award (10SDG2630103) from the American Heart Association. The authors would like to acknowledge Dr. Yuyu Sun and Dr. Daniel Engebretson for generously providing FTIR and SEM, respectively, for use in our experiments.

REFERENCES

- (1) Brunski, J. B. Metals. In *Biomaterials Science An Introduction to Materials in Medicine*, 2nd ed.; Ratner, B. D., Hoffman, A. S., Schoen, F. J., Lemons, J. E., Eds.; Elsevier Academic Press: London, 2004; pp 137–153.
- (2) Guehennec, L. L.; Soueidan, A.; Layrolle, P.; Amouriq, Y. Surface treatments of titanium dental implants for rapid osseointegration. *Dent. Mater.* **2007**, *23*, 844–854.
- (3) Alla, R. K.; Ginjupalli, K.; Upadhyay, N.; Shammas, M.; Ravi, R. K.; Sekhar, R. Surface roughness of implants: a review. *Trends Biomater. Artif. Organs* **2011**, *25*, 112–118.
- (4) Wen, X.; Wang, X.; Zhang, N. Microrough surface of metallic biomaterials: a literature review. *Biomed. Mater. Eng.* **1996**, *6*, 173–189.
- (5) Serruys, P. W.; Jaegere, P. D.; Kiemeneij, F.; Macaya, C.; Rutsch, W.; Heyndrickx, G.; Emanuelsson, H.; Marco, J.; Legrand, V.; Materne, P.; Belardi, J.; Sigwart, U.; Colombo, A.; Goy, J. J.; Heuvel, P. V. D.; Delcan, J.; Morel, M. A. A comparison of balloon-expandable-stent implantation with balloon angioplasty in patients with coronary artery disease. *N. Engl. J. Med.* **1994**, *331*, 489–495.
- (6) Fischman, D. L.; Leon, M. B.; Baim, D. S.; Schatz, R. A.; Savage, M. P.; Penn, I.; Detre, K.; Veltri, L.; Ricci, D.; Nobuyoshi, M.; Cleman, M.; Heuser, R.; Almond, D.; Teirstein, P. S.; Fish, R. D.; Colombo, A.; Brinker, J.; Moses, J.; Shaknovich, A.; Hirshfeld, J.; Bailey, S.; Ellis, S.; Rake, R.; Goldberg, S. A randomized comparison of coronary-stent placement and balloon angioplasty in the treatment of coronary artery disease. *N. Engl. J. Med.* **1994**, *331*, 496–501.
- (7) Holmes, J. State of the art in coronary intervention. *Am. J. Cardiol.* **2003**, *91*, 50A–53A.
- (8) Stone, G. W.; Ellis, S. G.; Cox, D. A.; Hermiller, J.; O’Shaughnessy, C.; Mann, J. T.; Turco, M.; Caputo, R.; Bergin, P.; Greenberg, J.; Popma, J. J.; Russell, M. E. A polymer-based, paclitaxel-eluting stent in patients with coronary artery disease. *N. Engl. J. Med.* **2004**, *350*, 221–231.
- (9) Morice, M. C.; Serruys, P. W.; Sousa, J. E.; Fajadet, J.; Hayashi, E. B.; Perin, M.; Colombo, A.; Schuler, G.; Barragan, P.; Guagliumi, G.; Molnar, F.; Falotico, R. A randomized comparison of a sirolimus-eluting stent with a standard stent for coronary revascularization. *N. Engl. J. Med.* **2002**, *346*, 1773–1780.
- (10) Finn, A. V.; Nakazawa, G.; Joner, M.; Kolodgie, F. D.; Mont, E. K.; Gold, H. K.; Virmani, R. Vascular responses to drug eluting stents: importance of delayed healing. *Arterioscler., Thromb., Vasc. Biol.* **2007**, *27*, 1500–10.
- (11) Ong, A. T. L.; McFadden, E. P.; Regar, E.; deJaegere, P. P. T.; vanDomburg, R. T.; Serruys, P. W. Late angiographic stent thrombosis (LAST) events with drug-eluting stents. *J. Am. Coll. Cardiol.* **2005**, *45*, 2088–2092.
- (12) Iakovou, I.; Schmidt, T.; Bonizzoni, E.; Ge, L.; Sangiorgi, G.; Stankovic, G.; Aioldi, F.; Chieffo, A.; Montorfano, M.; Carlino, M.; Michev, I.; Corvaja, N.; Briguori, C.; Gerckens, U.; Grube, E.; Colombo, A. Incidence, predictors, and outcome of thrombosis after successful implantation of drug-eluting stents. *JAMA* **2005**, *293*, 2126–2130.
- (13) McFadden, E. P.; Stabile, E.; Regar, E.; Cheneau, E.; Ong, A. T. L.; Kinnaird, T.; Suddath, W. O.; Weissman, N. J.; Torguson, R.; Kent, K. M.; Pichard, A. D.; Satler, L. F.; Waksman, R.; Serruys, P. W. Late thrombosis in drug-eluting coronary stents after discontinuation of antiplatelet therapy. *Lancet* **2004**, *364*, 1519–1521.
- (14) Joner, M.; Finn, A.; Farb, A.; Mont, E.; Kolodgie, F.; Ladich, E.; Kutys, R.; Skorija, K.; Gold, H.; Virmani, R. Pathology of drug-eluting stents in humans: delayed healing and late thrombotic risk. *J. Am. Coll. Cardiol.* **2006**, *48*, 203–205.
- (15) Heldman, A.; Cheng, L.; Jenkins, G.; Heller, P.; Kim, D.; Ware, M.; Nater, C.; Hruban, R.; Rezai, B.; Abella, B.; Bunge, K.; Kinsella, J.; Sollott, S.; Lakatta, E.; Brinker, J.; Hunter, W.; Froehlich, J. Paclitaxel stent coating inhibits neointimal hyperplasia at 4 weeks in a porcine model of coronary restenosis. *Circulation* **2001**, *103*, 2289–2295.
- (16) Wieneke, H.; Dirsch, O.; Sawitowski, T.; Gu, Y. L.; Brauer, H.; Dahmen, U.; Fischer, A.; Wnendt, S.; Erbel, R. Synergistic effects of a novel nanoporous stent coating and tacrolimus on intima proliferation in rabbits. *Catheter Cardiovasc. Interv.* **2003**, *60*, 399–407.
- (17) Kollum, M.; Farb, A.; Schreiber, R.; Terfera, K.; Arab, A.; Geist, A.; Haberstroh, J.; Wnendt, S.; Virmani, R.; Hehrlein, C. Particle debris from a nanoporous stent coating obscures potential antiproliferative effects of tacrolimus-eluting stents in a porcine model of restenosis. *Catheter Cardiovasc. Interv.* **2005**, *64*, 85–90.
- (18) Bhargava, B.; Reddy, N. K.; Karthikeyan, G.; Raju, R.; Mishra, S.; Singh, S.; Waksman, R.; Virmani, R.; Somaraju, B. A novel paclitaxel-eluting porous carbon-carbon nanoparticle coated, non-polymeric cobalt-chromium stent: evaluation in a porcine model. *Catheter Cardiovasc. Interv.* **2006**, *67*, 698–702.
- (19) Carter, A. J.; Wamhoff, B.; Brodeur, A.; Christians, U.; Tio, F.; Lye, W. K.; Owens, G. K. Pharmacokinetics and pharmacodynamics of stent-based delivery of sirolimus via a novel metallic anisotropic nanoporous surface coating. *Circulation* **2006**, *114*, II_511–II_512.
- (20) Costa, J. R.; Abizaid, A.; Costa, R.; Feres, F.; Tanajura, F.; Abizaid, A.; Maldonado, G.; Staico, R.; Siqueira, D.; Sousa, A. G.; Bonan, R.; Sousa, J. E. 1-year results of the hydroxyapatite polymer-free sirolimus-eluting stent for the treatment of single de novo coronary lesions: the VESTASYNC I trial. *JACC Cardiovasc. Interv.* **2009**, *2*, 422–427.
- (21) Wessely, R.; Hausleiter, J.; Michaelis, C.; Jaschke, B.; Vogeser, M.; Milz, S.; Behnisch, B.; Schratzenstaller, T.; Gluszko, M. R.; Stöver, M.; Wintermantel, E.; Kastrati, A.; Schöming, A. Inhibition of neointima formation by a novel drug-eluting stent system that allows for dose-adjustable, multiple, and on-site stent coating. *Arterioscler., Thromb., Vasc. Biol.* **2005**, *25*, 748–753.
- (22) Hausleiter, J.; Kastrati, A.; Wessely, R.; Dibra, A.; Mehilli, J.; Schratzenstaller, T.; Graf, I.; Gluszko, M. R.; Behnisch, B.; Dirschniger, J.; Wintermantel, E.; Schöming, A. Prevention of restenosis by a novel drug-eluting stent system with a dose-adjustable, polymer-free, on-site stent coating. *Eur. Heart J.* **2005**, *26*, 1475–1481.
- (23) Garg, S.; Serruys, P. W. Coronary stents current status. *J. Am. Coll. Cardiol.* **2010**, *56*, S1–S42.
- (24) Song, D.; Hsu, L. F.; Au, J. L. Binding of taxol to plastic and glass containers and protein under in vitro conditions. *J. Pharm. Sci.* **1996**, *85*, 29–31.
- (25) Lee, B. H.; Nam, H. Y.; Kwon, T.; Kim, S. J.; Kwon, G. Y.; Jeon, H. J.; Lim, H. J.; Lee, W. K.; Park, J.-s.; Ko, J. Y.; Kim, D. J. Paclitaxel-coated expanded polytetrafluoroethylene haemodialysis grafts inhibit neointimal hyperplasia in porcine models of graft stenosis. *Nephrol., Dial., Transplant.* **2006**, *21*, 2432–2438.
- (26) Mani, G.; Macias, C. E.; Feldman, M. D.; Marton, D.; Oh, S.; Agrawal, C. M. Delivery of paclitaxel from cobalt–chromium alloy surfaces without polymeric carriers. *Biomaterials* **2010**, *31*, 5372–5384.
- (27) Mani, G.; Torres, N.; Oh, S. Paclitaxel delivery from cobalt–chromium alloy surfaces using self-assembled monolayers. *Biointerphases* **2011**, *6*, 33–42.
- (28) Lu, J.; Rao, M. P.; MacDonald, N. C.; Khang, D.; Webster, T. J. Improved endothelial cell adhesion and proliferation on patterned titanium surfaces with rationally designed, micrometer to nanometer features. *Acta Biomater.* **2008**, *4*, 192–201.

- (29) Lu, J.; Khang, D.; Webster, T. J. Greater endothelial cell responses on submicron and nanometer rough titanium surfaces. *J. Biomed. Mater. Res., Part A* **2010**, *94*, 1042–1049.
- (30) Lampin, M.; Clérout, R. W.; Legris, C.; Degrange, M.; Luizard, M. F. S. Correlation between substratus roughness and wettability, cell adhesion, and cell migration. *J. Biomed. Mater. Res.* **1996**, *36*, 99–108.
- (31) Yazdani, S. K.; Kolodgie, F. D.; Virmani, R. Ex vivo and preclinical assessment of an endothelial progenitor cell capturing bioengineered stent. *Minerva Cardioangiologica*. **2012**, *60*, 11–22.
- (32) Rognoni, A.; Secco, G. G.; Lupi, A.; Santagostino, M.; Sansa, M.; Bongo, A. S.; Rognoni, G. Use of endothelial progenitor capture cell stent during percutaneous treatment of coronary bifurcations: a prospective angiographic registry. *Crit. Pathways Cardiol.* **2011**, *10*, 189–192.
- (33) Park, J. Y.; Gemmell, C. H.; Davies, J. E. Platelet interactions with titanium: modulation of platelet activity by surface topography. *Biomaterials* **2001**, *22*, 2671–2682.
- (34) Kikuchi, L.; Park, J. Y.; Victor, C.; Davies, J. E. Platelet interactions with calcium-phosphate-coated surfaces. *Biomaterials* **2005**, *26*, 5285–5295.
- (35) Chepurov, A. K.; Mertsalova, N. N. Interrelationship between contact coagulation, surface charge and roughness. *Fiziol. Zh. SSSR im. I. M. Sechenova* **1978**, *64*, 1559–1567.
- (36) Dobrovolskaia, M. A.; Patri, A. K.; Simak, J.; Hall, J. B.; Semberova, J.; Lacerda, S. H. D. P.; McNeil, S. E. Nanoparticle size and surface charge determine effects of PAMAM dendrimers on human platelets in vitro. *Mol. Pharm.* **2012**, *9*, 382–93.
- (37) Sagnella, S.; Ngam, K. M. Chitosan based surfactant polymers designed to improve blood compatibility on biomaterials. *Colloids Surf., B* **2005**, *42*, 147–155.
- (38) Sarkar, S.; Sales, K. M.; Hamilton, G.; Seifalian, A. M. Addressing thrombogenicity in vascular graft construction. *J. Biomed. Mater. Res., Part B* **2007**, *82*, 100–108.
- (39) Taga, Y.; Kawai, K.; Nokubi, T. New method for divesting cobalt-chromium alloy castings: sandblasting with a mixed abrasive powder. *J. Prosthet. Dent.* **2001**, *85*, 357–362.
- (40) Sipos, L.; Som, A.; Faust, R.; Richard, R.; Schwarz, M.; Ranade, S.; Boden, M.; Chan, K. Controlled delivery of paclitaxel from stent coatings using poly(hydroxystyrene-b-isobutylene-b-hydroxystyrene) and its acetylated derivative. *Biomacromolecules* **2005**, *6*, 2570–2582.
- (41) Kim, T. G.; Lee, H.; Jang, Y.; Park, T. G. Controlled release of paclitaxel from heparinized metal stent fabricated by layer-by-layer assembly of polylysine and hyaluronic acid-g-poly(lactic-co-glycolic acid) micelles encapsulating paclitaxel. *Biomacromolecules* **2009**, *10*, 1532–1539.
- (42) Lim, H. J.; Nam, H. Y.; Lee, B. H.; Kim, D. J.; Ko, J. Y.; Park, J. S. A novel technique for loading of paclitaxel-PLGA nanoparticles onto ePTFE vascular grafts. *Biotechnol. Prog.* **2007**, *23*, 693–697.
- (43) Innocente, F.; Mandracchia, D.; Pektok, E.; Nottelet, B.; Tille, J. C.; Valence, S. D.; Faggian, G.; Mazzucco, A.; Kalangos, A.; Gurny, R.; Moeller, M.; Walpeth, B. H. Paclitaxel-eluting biodegradable synthetic vascular prostheses: a step towards reduction of neointima formation? *Circulation* **2009**, *120*, S37–S45.
- (44) Raman, A.; Bubey, M.; Gouzman, I.; Gawalt, E. S. Formation of self-assembled monolayers of alkylphosphonic acid on the native oxide surface of SS316L. *Langmuir* **2006**, *22*, 6469–6472.
- (45) Quinones, R.; Gawalt, E. S. Study of the formation of self-assembled monolayers on nitinol. *Langmuir* **2007**, *23*, 10123–10130.
- (46) Quinones, R.; Raman, A.; Gawalt, E. Functionalization of nickel oxide using alkylphosphonic acid self-assembled monolayers. *Thin Solid Films* **2008**, *S16*, 8774–8781.
- (47) Mani, G.; Feldman, M. D.; Oh, S.; Agrawal, C. M. Surface modification of cobalt–chromium–tungsten–nickel alloy using octadecyltrichlorosilanes. *Appl. Surf. Sci.* **2009**, *255*, 5961–5970.
- (48) Raman, A.; Dubey, M.; Gouzman, I.; Gawalt, E. S. Formation of self-assembled monolayers of alkylphosphonic acid on the native oxide surface of SS316L. *Langmuir* **2006**, *22*, 6469–6472.
- (49) Raman, A.; Gawalt, E. S. Self-assembled monolayers of alkanoic acids on the native oxide surface of SS316L by solution deposition. *Langmuir* **2007**, *23*, 2284–2288.
- (50) Otsuka, Y.; Chronos, N.; Apkarian, R.; Robinson, K. Scanning electron microscopic analysis of defects in polymer coatings of three commercially available stents: comparison of biodivYsio, taxus and cypher stents. *J. Invasive Cardiol.* **2007**, *19*, 71–76.
- (51) Basalus, M. W.; Ankone, M. J.; Houwelingen, G. K. v.; Man, F. H. d.; Birgelen, C. v. Coating irregularities of durable polymer-based drug-eluting stents as assessed by scanning electron microscopy. *Eurointervention* **2009**, *5*, 157–165.
- (52) Wiemer, M.; Butz, T.; Schmidt, W.; Schmitz, K. P.; Horstkotte, D.; Langer, C. Scanning electron microscopic analysis of different drug eluting stents after failed implantation: from nearly undamaged to major damaged polymers. *Catheter Cardiovasc. Interv.* **2010**, *75*, 905–911.
- (53) Basalus, M. W.; Tandjung, K.; Westen, T. v.; Sen, H.; Jagt, P. K. v. d.; Grijpma, D. W.; Apeldoorn, A. A. v.; Birgelen, C. v. Scanning electron microscopic assessment of coating irregularities and their precursors in unexpanded durable polymer-based drug-eluting stents. *Catheter Cardiovasc. Interv.* **2012**, *79*, 644–653.
- (54) Virmani, R.; Guagliumi, G.; Farb, A.; Musumeci, G.; Grieco, N.; Motta, T.; Mihalcsik, L.; Tespili, M.; Valsecchi, O.; Kolodgie, F. Localized hypersensitivity and late coronary thrombosis secondary to a sirolimus-eluting stent: should we be cautious? *Circulation* **2004**, *109*, 701–705.
- (55) Virmani, R.; Kolodgie, F.; Farb, A. Drug-eluting stents: are they really safe? *Am. Heart Hosp. J.* **2004**, *2*, 85–88.
- (56) Virmani, R.; Farb, A.; Guagliumi, G.; Kolodgie, F. Drug-eluting stents: caution and concerns for long-term outcome. *Coron. Artery Dis.* **2004**, *15*, 313–318.
- (57) Nebeker, J. R.; Virmani, R.; Bennet, C. L.; Hoffman, J. M.; Samore, M. H.; Alvarez, J.; Davidson, C. J.; McKoy, J. M.; Raish, D. W.; Whisenant, B. K.; Yarnold, P. R.; Belknap, S. M.; West, D. P.; Gage, J. E.; Morse, R. E.; Gligoric, G.; Davidson, L.; Feldman, M. D. Hypersensitivity cases associated with drug-eluting coronary stents: a review of available cases from the research on adverse drug events and reports (RADAR) project. *J. Am. Coll. Cardiol.* **2006**, *47*, 182–183.
- (58) Mani, G.; Feldman, M. D.; Patel, D.; Agrawal, C. M. Coronary stents: a materials perspective. *Biomaterials* **2007**, *28*, 1689–1710.
- (59) Russ, J. C. *The Image Processing Handbook*, 6th ed.; CRC Press Taylor & Francis Group, LLC: Boca Raton, FL, 2011.
- (60) Losic, D.; Shapter, J. G.; Gooding, J. J. Influence of surface topography on alkanethiol SAMs assembled from solution and by microcontact printing. *Langmuir* **2001**, *17*, 3307–3316.
- (61) Creager, S. E.; Hockett, L. A.; Rowe, G. K. Consequences of microscopic surface roughness for molecular self-assembly. *Langmuir* **1992**, *8*, 854–861.
- (62) Douglass, E. F.; Driscoll, P. F.; Liu, D.; Burnham, N. A.; Lambert, C. R.; McGimpsey, W. G. Effect of electrode roughness on the capacitive behavior of self-assembled monolayers. *Anal. Chem.* **2008**, *80*, 7670–7677.
- (63) Chockalingam, M.; Darwish, N.; Saux, G. L.; Gooding, J. J. Importance of indium tin oxide substrate on the quality of self-assembled monolayers formed from organophosphonic acids. *Langmuir* **2011**, *27*, 2545–2552.
- (64) Dhanikula, A. B.; Panchagnula, R. Development and characterization of biodegradable chitosan films for local delivery of paclitaxel. *AAPS J.* **2004**, *6*, 1–12.
- (65) Lee, B. H.; Lee, J. E.; Lee, K. W.; Nam, H. Y.; Jeon, H. J.; Sung, Y. J.; Kim, J. S.; Lim, H. J.; Park, J. S.; Ko, J. Y.; Kim, D. J. Coating with paclitaxel improves graft survival in a porcine model of haemodialysis graft stenosis. *Nephrol., Dial., Transplant.* **2007**, *22*, 2800–2804.
- (66) Baek, I.; Bai, C. Z.; Hwang, J.; Nam, H. Y.; Park, J. S.; Kim, D. J. Paclitaxel coating of the luminal surface of hemodialysis grafts with effective suppression of neointimal hyperplasia. *J. Vasc. Surg.* **2012**, *55*, 806–814.

- (67) Kamath, K.; Barry, J. J.; Miller, K. M. The taxus drug-eluting stent: a new paradigm in controlled drug delivery. *Adv. Drug Delivery Rev.* **2006**, *58*, 412–436.
- (68) Kang, Y.; Wu, J.; Yin, G.; Huang, Z.; Liao, X.; Yao, Y.; Ouyang, P.; Wang, H.; Yang, Q. Characterization and biological evaluation of paclitaxel-loaded poly(L-lactic acid) microparticles prepared by supercritical CO₂. *Langmuir* **2008**, *24*, 7432–7441.
- (69) Danhier, F.; Lecouturier, N.; Vroman, B.; Jérôme, C.; Brynaert, J. M.; Feron, O.; Préat, V. Paclitaxel-loaded PEGylate PLGA-based nanoparticles: in vitro and in vivo evaluation. *J. Controlled Release* **2009**, *133*, 11–17.
- (70) Jin, C.; Bai, L.; Wu, H.; Song, W.; Guo, G.; Dou, K. Cytotoxicity of paclitaxel incorporated in PLGA nanoparticles on hypoxic human tumor cells. *Pharm. Res.* **2009**, *26*, 1776–1784.
- (71) Donyai, P.; Sewell, G. J. Physical and chemical stability of paclitaxel infusions in different container types. *J. Oncol. Pharm. Pract.* **2006**, *12*, 211–222.
- (72) Tian, J.; Stella, V. J. Degradation of paclitaxel and related compounds in aqueous solutions I: epimerization. *J. Pharm. Sci.* **2008**, *97*, 1224–1235.
- (73) Tian, J.; Stella, V. J. Degradation of paclitaxel and related compounds in aqueous solutions II: Nonepimerization degradation under neutral to basic pH conditions. *J. Pharm. Sci.* **2008**, *97*, 3100–3108.
- (74) Palmgren, J. J.; Monkkonen, J.; Korjamo, T.; Hassinen, A.; Auriola, S. Drug adsorption to plastic containers and retention of drugs in cultured cells under *in vitro* conditions. *Eur. J. Pharm. Biopharm.* **2006**, *64*, 369–378.
- (75) Jabara, R.; Chronos, N.; Conway, D.; Molema, W.; Robinson, K. Evaluation of a novel slow-release paclitaxel-eluting stent with a bioabsorbable polymeric surface coating. *JACC Cardiovasc. Interv.* **2008**, *1*, 81–87.
- (76) Kozuki, A.; Shite, J.; Shinke, T.; Miyoshi, N.; Sawada, T.; Hellig, F.; Abelson, M.; Brown, B.; Khan, S.; Mpe, M.; Ntsekhe, M.; Conway, D.; Hirata, K. STELLIUM 1: first-in-man follow-up evaluation of bioabsorbable polymer-coated paclitaxel-eluting stent. *Circ. J.* **2010**, *74*, 2089–2096.
- (77) Serruys, P. W.; Sianos, G.; Abizaid, A.; Aoki, J.; Heijer, P. d.; Bonnier, H.; Smits, P.; McClean, D.; Verheyen, S.; Belardi, J.; Condado, J.; Pieper, M.; Gambone, L.; Bressers, M.; Symons, J.; Sousa, E.; Litvack, F. The effect of variable dose and release kinetics on neointimal hyperplasia using a novel paclitaxel-eluting stent platform: the paclitaxel in-stent controlled elution study (PISCES). *J. Am. Coll. Cardiol.* **2005**, *46*, 253–260.